Interaction cross sections and structure of light exotic nuclei

O. M. Knyaz'kov
St. Petersburg State University

I. N. Kukhtina
Joint Institute for Nuclear Research, Dubna

S. A. Fayans
Kurchatov Institute, Moscow

Fiz. Élem. Chastits At. Yadra **30**, 870–907 (July–August 1999)

The recent experimental data on the total reaction cross sections and the interaction cross sections for light exotic nuclei are reviewed. The various approaches—phenomenological and semi-microscopic—to calculating these quantities are described. The rms radii of the neutron, proton, and matter distributions extracted from comparison with the data are analyzed for a large group of nuclei. Possible candidates for nuclei with a neutron or proton halo are discussed. New experiments involving light exotic nuclei are proposed. © *1999 American Institute of Physics.* [S1063-7796(99)00204-1]

INTRODUCTION

The widespread use of radioactive beams during the last 15 years has led to the establishment of a number of unusual properties of light exotic nuclei, i.e., nuclei far from the β-stability line but with characteristics greatly differing from those predicted by the systematics (see, for example, Refs. 1–7 and references therein). One of the most important characteristics of the interaction of light exotic nuclei with stable target nuclei is the interaction cross section σ_I or the total reaction cross section σ_R. The experimental study of light nuclei in fact began with the measurement of σ_I in the pioneering work of Tanihata *et al.*[8] On the basis of analysis of the measured interaction cross sections for He, Li, and Be isotopes at energy 790 MeV/nucleon using both the empirical approach and the Glauber approximation, it was concluded[8–11] that the neutron density in neutron-rich isotopes of these nuclei is quite extended. This led to the hypothesis that a neutron halo may exist in some of them. Further studies showed that a neutron halo can actually be realized in ^{6}He, ^{11}Li, and ^{11}Be. Hints of the existence of an analogous phenomenon in ^{8}B, a nucleus with a proton excess, were found in Ref. 12. Subsequent measurements of σ_I were performed both for an extended energy range of the projectile and for an extended range of mass numbers. The total reaction cross sections σ_R at intermediate energies ($E/A<100$ MeV/nucleon) were measured in several studies.[13–17] The first such measurements were performed in Ref. 13, where the total reaction cross sections for ^{8}He, ^{9}Li, and other exotic nuclei at energy 30–40 MeV/nucleon were obtained. For the isotopes ^{8,9,11}Li the cross sections σ_R were measured at 80 MeV/nucleon in Refs. 14 and 15, and for ^{4,6,8}He, $^{6-9,11}$Li, ^{10}Be, and ^{8}B they were measured at 20 to 60 MeV/nucleon in Refs. 16 and 17. Measurements of the total reaction cross sections for ^{8}B in the range from 10 to 40 MeV/nucleon were made in Ref. 18. Parallel studies were carried out at high projectile energies. The interaction cross sections for ^{15}B, ^{9,10,15}C, ^{13}N, and ^{14,15}O at 730 MeV/nucleon were measured in Ref. 19, and repeat measurements of σ_I for ^{8}B were performed at 790 MeV/nucleon in Ref. 20. In most cases the measurements were performed on a carbon or silicon target.

In recent years, measurements of the cross sections for light exotic nuclei interacting with stable nuclei have not been limited to isotopes of He, Li, Be, and B, but have been extended to heavier nuclei. The cross sections σ_I for Na isotopes with mass numbers $A=20-23$ and $A=25-32$ were measured in Ref. 21. Analysis of these experimental data led to the hypothesis[21,22] that a neutron halo exists also in Na isotopes possessing a large neutron excess. After ^{8}B, neutron-deficient isotopes of phosphorous were considered as candidates for nuclei with a proton halo. Experimental study of the ^{26,27}P isotopes, including measurement of the total reaction cross sections at 65 MeV/nucleon,[23] qualitatively confirmed the hypothesis[24] that a proton halo exists in these nuclei. Measurements of σ_R for neutron-rich unstable nuclei of the $f-p$ shell at 50–70 MeV/nucleon were performed in Ref. 25. Analysis of those data revealed an important dependence of the cross sections and, accordingly, the matter distribution radii in these nuclei, on the ratio of the numbers of neutrons and protons. This makes it extremely important to measure the interaction cross sections for chains of isobar nuclei. Such measurements were carried out in Ref. 26 for isobars with $A=17$ at 700 MeV/nucleon, and in Ref. 27 for isobars with $A=20$ at 950 MeV/nucleon. In this review of the experiments we have restricted ourselves to the main studies and make no claim of completeness.

The experimental data on $\sigma_I(\sigma_R)$ are, as a rule, analyzed using three basic approaches: the empirical approach, the optical model, and the Glauber theory.[28] In the empirical approach one uses either geometrical representations of the high-energy interaction of two colliding nuclei,[8] or the strong-absorption model, in which the cross sections are parametrized in accordance with the Kox formula[29] or a modification of it. In most cases the standard optical model turns

out to be inapplicable for describing the interaction of light exotic nuclei with stable nuclei, and so a semi-microscopic version of it is used,[30] in which the input data for calculating the cross sections are the matter distribution densities in the colliding nuclei and the effective nucleon–nucleon forces. The approach most popular for analyzing the experimental data on the interaction cross sections is that based on the Glauber approximation. The first such analysis was performed in Ref. 9. The basic information extracted from the experimental cross sections is the strong-absorption radii (in the empirical approach) and the rms radii of the matter, neutron, and proton distributions in semi-microscopic approaches (the folding model and the Glauber approximation). In this case, when the densities are calculated using nuclear-structure models, it becomes possible to test these models by comparing the experimental cross sections with the theoretical ones. Various approaches have been used to calculate the nuclear densities. One of them is the density-functional method,[31] which is used to calculate the neutron and proton densities for both the target nucleus and the projectile on a common basis.

This review is devoted to the analysis of the principal experimental data on the interaction cross sections (total reaction cross sections) of light exotic nuclei. In Sec. 1 we present the theoretical approaches to the construction of the cross sections: the empirical approach, including the Kox parametrization, various versions of the folding model, and the Glauber approximation and its application to the analysis of experimental data at intermediate and high energies. In Sec. 2 we present the experimental interaction cross sections for isotopes of He, Li, Be, B, and Na and isobars with $A=17$ and $A=20$, and analyze them. The features of the neutron and proton distributions in these nuclei are discussed, along with the possibilities offered by nuclear-structure models. In the Conclusion we review the main results and discuss further possibilities for studying the properties of light exotic nuclei using experiments to measure the interaction cross sections and to study nuclear reactions with unstable nuclei.

1. THEORETICAL MODELS

1.1. Parametrization of the cross sections

On the basis of geometrical arguments about the interaction of two colliding nuclei at high energies, the interaction cross section can be written as

$$\sigma_I(p,t)=\pi[R_I(p)+R_I(t)]^2. \tag{1}$$

Here and below, the letters p and t refer to the projectile and the target nucleus. Knowing $R_I(t)$ from the description of the interaction of stable nuclei, it is possible to determine $R_I(p)$ by using (1) and comparing $\sigma_I(p,t)$ with the value of σ_I obtained experimentally. The deviation of the behavior of $R_I(p)$ for light exotic nuclei from the $A^{1/3}$ law was first found in this way.[8,9] The representation (1) is the simplest representation for σ_I, and neglects many factors.

A more realistic parametrization of the interaction cross sections, the Kox parametrization, was proposed in Ref. 29:

$$\sigma_I=\pi r_0^2\left(A_p^{1/3}+A_t^{1/3}+a\cdot\frac{A_p^{1/3}\cdot A_t^{1/3}}{A_p^{1/3}+A_t^{1/3}}-C(E)\right)^2\left(1-\frac{B}{E_{\rm cm}}\right). \tag{2}$$

Here A_p and A_t are the mass numbers, B is the energy of the Coulomb barrier, and $E_{\rm cm}$ is the energy of the colliding nuclei in the center-of-mass frame. The parameter a and also the numerical values of $C(E)$ are determined by analyzing the interaction of stable nuclei in a wide energy range. In a first approximation the Coulomb barrier can be calculated by studying the interaction of two charged spheres. A more complicated parametrization for B was suggested in Ref. 32. In contrast to (1), the approximation of separability in the projectile and the target nucleus was not used in constructing (2), but Coulomb effects and the energy dependence are taken into account. Therefore, Eq. (2) is more universal, since it can be used at both high and low energies. Comparison of the cross section σ_R calculated using (2) with the experimental value allows the determination of r_0, which, in accordance with the strong-absorption model, is interpreted as the parameter corresponding to the strong-absorption radius. The values of r_0 for many light exotic nuclei have been determined in this way.

Parametrizations of σ_R even more complicated than (2) are also used (see, for example, Ref. 18). They take into account the difference between the strong-absorption radii for the projectile and the target nucleus, and an additional energy dependence $\propto E_{cm}^{-1/3}$ is introduced, along with dependence on the numbers of protons and neutrons in the colliding nuclei.

Analysis of the experimental cross sections on the basis of parametrizations like (2) allows the general geometrical properties of light nuclei and the potentials for their interaction with stable nuclei to be established, but does not permit determination of the nuclear matter distributions and, in particular, does not explain the differences between the proton and neutron distributions.

1.2. The macroscopic optical model

The standard optical potential of the phenomenological optical model has the form

$$U_{\rm opt}(r)=-V_Rf_R(r)-iW_vF_I(r)+4ia_IW_s(d/dr)f_I(r)+2(\pi/m_\pi c)^2\cdot\frac{1}{r}\cdot(d/dr)V_{Ls}f_s(r)(\mathbf{L}\cdot\mathbf{S})+V_{\rm coul}(r), \tag{3}$$

$$R_i=r_iA^{1/3},\quad f_i=(1+\exp((r-R_i)/a_i))^{-1},\quad i=R,I,LS. \tag{3a}$$

Here the first term is the central part of the real potential, the second and third terms are the exchange and surface-absorption potentials, and the next term is the spin–orbit term. The last term in (3) is usually taken to be the Coulomb interaction of two charged spheres.

The potential $U_{\rm opt}(r)$ can be used to construct the S-matrix elements and the total reaction cross section in the standard way:

$$\sigma_R=\frac{\pi}{k^2}\sum_l (2l+1)(1-|S_l|^2). \quad (4)$$

Here the summation runs over all the reaction channels. We note that at high energies it is not σ_R which is measured experimentally, but the interaction cross section σ_I. The differences between σ_R and σ_I are due to the contribution of inelastic scattering. It is estimated that these differences are 5–10% at high energies. The cross section σ_R is calculated theoretically (both in the optical model and in the Glauber approximation), which should be borne in mind when comparing the calculated interaction cross sections with the experimental ones at high energies.

Equation (3) contains many parameters (from nine to twelve), and so calculations of σ_R in the microscopic optical model can possess predictive power only when the parameters of the optical potential are determined by analyzing the corresponding angular distributions of elastic scattering. Unfortunately, so far there have been few measurements in which both σ_R and the differential cross sections of elastic scattering for light exotic nuclei have been obtained simultaneously. On the other hand, for such nuclei the microscopic optical model rarely leads to a successful description of the experimental data (see Ref. 7 and references therein). This is because the radial dependence of all the form factors in (3) is fixed as a Woods–Saxon dependence, whereas already for nucleons and α particles it has been shown[33,34] that the potential constructed on the basis of the effective forces differs from the Woods–Saxon form. Therefore, the microscopic optical model has been used only in certain cases for analyzing σ_R for light exotic nuclei.[16,35–37]

1.3. The semi-microscopic optical model

In several studies,[18,35,39–41] σ_R has been analyzed using double-folding potentials within the semi-microscopic optical model. Such potentials for describing the interaction of two composite particles are constructed as follows. In first order in the effective forces, the interaction potential of two colliding nuclei can be written as the sum

$$U(\mathbf{R})=U^E(\mathbf{R})+U^D(\mathbf{R}), \quad (5)$$

where $U^D(\mathbf{R})$ is the direct potential of the double-folding model:[42]

$$U^D(\mathbf{R})=\int\int \rho^{(1)}(\mathbf{r}_1)V^D(\mathbf{s})\rho^{(2)}(\mathbf{r}_2)d\mathbf{r}_1 d\mathbf{r}_2. \quad (6)$$

Here $V^D(\mathbf{s})$ is the direct component of the effective interaction, $\mathbf{s}=\mathbf{r}_2-\mathbf{r}_1+\mathbf{R}$, and $\rho^{(i)}(\mathbf{r}_i)$ are the densities of the colliding nuclei ($i=1,2$). The main contribution to the exchange potential $U^E(\mathbf{R})$ comes from one-nucleon exchange effects, which can be described in the density-matrix formalism:[43]

$$U^E(\mathbf{R})=\int\int \rho^{(1)}(\mathbf{r}_1,\mathbf{r}_1+\mathbf{s})V_E(\mathbf{s})\rho^{(2)}(\mathbf{r}_2,\mathbf{r}_2-\mathbf{s}) \times\exp(i\mathbf{k}(\mathbf{R})\mathbf{s}/\eta)d\mathbf{r}_1 d\mathbf{r}_2. \quad (7)$$

This is the localized form of the exchange term. Here $V_E(\mathbf{s})$ is the exchange component of the effective interaction, $\rho^{(i)}(\mathbf{r},\mathbf{r}')$ ($i=1,2$) is the density matrix of the colliding nuclei ($i=1,2$), $\mathbf{k}(\mathbf{R})$ is the local momentum, given by

$$k^2(\mathbf{R})=(2m\eta/\hbar^2)(E-U(\mathbf{R})-V_c(\mathbf{R})), \quad (8)$$

where

$$\eta=\frac{A_1A_2}{A_1+A_2}, \quad (8a)$$

A_i ($i=1,2$) are the nuclear mass numbers, and $V_c(\mathbf{R})$ is the Coulomb potential. The scheme for calculating $U^E(R)$ is described in detail in, for example, Ref. 7.

It follows from (6) and (7) that the input data for calculating the double-folding potentials are the effective nucleon–nucleon forces and the density matrices of the colliding nuclei, where the latter can be reduced to densities diagonal in the coordinate representation by using the formalism of expansion of the density matrix.[44]

The effective nucleon–nucleon forces are usually taken to be the M3Y effective interactions, based on the G-matrix elements of the Reid–Elliott potential[45] or the Paris potential.[46] The interaction of stable nuclei is also described by M3Y interactions depending on the matter distribution density in the nuclei (see Ref. 47 and references therein), where the density dependence is taken into account in the form of the factor

$$V(\mathbf{s},\rho)=V(\mathbf{s})F(\rho). \quad (9)$$

However, the choice of this factor noticeably affects only the angular distributions of elastic scattering at intermediate angles. Unfortunately, the angular distributions for light exotic nuclei have been obtained only up to 20° and, as shown in Ref. 48, they are insensitive to the choice of $F(\rho)$. Moreover, the density dependence of the effective forces weakly affects σ_R. Therefore, at this stage to analyze σ_R for light exotic nuclei it appears reasonable to use density-independent effective forces in (6) and (7).

The complete M3Y interaction, i.e., the exchange and direct, isoscalar and isovector components, is used to explicitly include one-nucleon exchange effects. There is an approximate version of the use of M3Y forces in which, in order to effectively include the Pauli principle, the exchange term is replaced by a zero-range pseudopotential[30] taking into account the density-dependence factor $F(\rho)$ (Ref. 49), added to the direct component $V^D(\mathbf{s})$. The corresponding interaction is called the DDM3Y interaction. An alternative to the DDM3Y interaction is the JLM interaction,[50] in which the effects of Pauli forbiddeness are also included implicitly. In addition, that interaction contains an imaginary part, which in folding models leads to a complex optical potential. Approximate versions of the double-folding model have been used to analyze the interaction of light exotic nuclei with stable nuclei.[18,35,38]

The scheme for calculating the potentials involves the nucleon densities in addition to the effective nucleon–nucleon forces. To calculate the potentials in the isoscalar and isovector channels, it is convenient to introduce the isoscalar and isovector densities:

$$\rho_0^{(i)}(\mathbf{r})=\rho_n^{(i)}(\mathbf{r})+\rho_p^{(i)}(\mathbf{r}), \quad (10)$$

$$\rho_1^{(i)}(\mathbf{r})=\rho_n^{(i)}(\mathbf{r})-\rho_p^{(i)}(\mathbf{r}). \quad (11)$$

The proton and neutron densities can be parametrized or calculated by using nuclear-structure models. In the latter case, comparison of the calculated cross sections σ_R with the experimental data allows the nuclear models describing the structure of light exotic nuclei to be tested.

The full optical potential must include an imaginary part as well as a real part. The former is responsible for the absorption of the incident particle in inelastic channels. There are three basic methods for including the absorption potential in the semi-microscopic optical model. In the first, the standard form of the imaginary part of the optical potential with radial Woods–Saxon dependence is used:

$$W^{(1)}(R)=W_{WS}(R), \quad (12)$$

where the right-hand side can contain both a volume and a surface term [see (3)]. In this case the scheme for analyzing the experimental data contains many fitted parameters, which can introduce uncertainty into the results. Another approach is to choose the absorption potential to be proportional to the calculated real part:

$$W^{(2)}(R)=iN_W U(R), \quad (13)$$

where N_W is the only fitted parameter in the absorption potential. However, Eq. (13) implies that the geometry of the real and imaginary parts of the potential is the same, which may not correspond to physical reality. It has therefore been proposed that the following expression be used for the imaginary part of the optical potential:[39]

$$W^{(3)}(R)=i\left(N_W U(R)-\alpha_W R\frac{dU(R)}{dR}\right), \quad (14)$$

where $U(R)$ is the double-folding potential (5), and N_W and α_W are parameters respectively characterizing the volume and surface parts of the absorption potential. In order for the calculations of the reaction cross sections using the potentials (5) and (14) to possess predictive power, it is necessary, as noted at the end of the preceding section, to determine the parameters N_W and α_W either from analysis of the angular distributions of elastic scattering, or from the systematics of the imaginary part of the optical potential, using the corresponding neighboring isotopes.

In the multichannel theory of nuclear reactions, the absorption potential forms a part of the dynamical polarization potential.[47] The latter also has a real part, which is important for describing the angular distributions of elastic scattering,[51] but only insignificantly affects σ_R, and so it can be neglected in analyzing the total reaction cross sections by the real part of the optical potential.

1.4. The Glauber approximation

At high interaction energies the sum in (4) can be replaced by an integral over the impact parameter. As a result we find

$$\sigma_R=2\pi\int_0^\infty db\cdot b\cdot[1-T(b)], \quad (15)$$

$$T(b)=|S(b)|^2. \quad (16)$$

At intermediate and high energies the optical limit of the Glauber theory is a good approximation.[28] In this case $T(b)$ has the form

$$T(b)=\exp\left[-\bar{\sigma}_{NN}\cdot\int\alpha^2\mathbf{b}_1\rho_z^{(1)}(\mathbf{b}_1)\rho_z^{(2)}(|\mathbf{b}_1-\mathbf{b}|)\right], \quad (17)$$

$$\bar{\sigma}_{NN}=\frac{N_pN_t\sigma_{nn}+Z_pZ_t\sigma_{pp}+N_pZ_t\sigma_{np}+N_tZ_p\sigma_{np}}{A_pA_t}, \quad (18)$$

$$\rho_z^{(i)}(\mathbf{b})=\int_{-\infty}^{+\infty}dz\rho_i((b^2+z^2)^{1/2}) \quad (i=1,2). \quad (19)$$

Equations (15) and (17)–(19) can be used to calculate σ_R on the basis of information about the averaged cross sections of nucleon–nucleon scattering and the nuclear densities. The energy dependence of σ_{nn} and σ_{np} ($\sigma_{pp}=\sigma_{nn}$) is well known and parametrized. The parameterization proposed in Ref. 52 is most common. If the densities are parametrized, then by comparing the theoretical and experimental cross sections it is possible to extract information about the parameters which are used. In the case where the densities are calculated, it is possible to test nuclear-structure models. Equations (15) and (17)–(19) do not contain free parameters, and therefore have an advantage over the optical-model expressions for calculating σ_R. However, Eq. (17) gives σ_R in the approximation of zero nucleon–nucleon interaction range and does not include many other factors. Let us consider these factors.

It is pointed out in Ref. 53 that a more realistic expression for $T(b)$ is one containing a function responsible for the finite range of the nucleon–nucleon interaction. When this function is introduced, $T(b)$ takes the form

$$T(b)=\exp\left[-\bar{\sigma}_{NN}\cdot\int d^2\mathbf{b}_1\int d^2\mathbf{b}_2 f(|\mathbf{b}_1-\mathbf{b}_2|)\times\rho_z^{(1)}(\mathbf{b}_1)\rho_z^{(2)}(|\mathbf{b}_2-\mathbf{b}|)\right]. \quad (20)$$

The function $f(|\mathbf{b}_1-\mathbf{b}_2|)$ is a Gaussian with parameter a. In accordance with the two-particle t matrix,[54] the value $a=1$ F was used in Ref. 53. In the limit $a\to 0$ (zero range), $f(|\mathbf{b}_1-\mathbf{b}_2|)$ becomes a δ function, and Eq. (20) becomes (17). The inclusion of finite range in (20) leads to a $\sim 8\%$ increase of the calculated cross sections.[53]

Equations (17) and (20) are valid assuming that the forward nucleon–nucleon scattering amplitude is purely imaginary, which may not be true even at high energies.[55] Accordingly, a complex expression is used for $\bar{\sigma}_{NN}$ (Ref. 56):

$$\bar{\sigma}_{NN}\to\bar{\sigma}_{NN}(i+\alpha_{NN}). \quad (21)$$

Here α_{NN} is a parameter characterizing the ratio of the real and imaginary parts of the forward NN scattering amplitude. As shown in Ref. 57, the cross section changes insignificantly (by only 8 mb) when the value of α_{NN} from Ref. 55 is used.

For light exotic nuclei with a neutron or proton excess, effects related to differences in the neutron and proton distributions in the nucleus can be important. In this case, in

(17) or (20) the averaged cross section $\bar{\sigma}_{NN}$ must be replaced by σ_{nn} and σ_{np} at the corresponding energy, and the difference between the neutron and proton densities must be taken into account. Here the expression for $T(b)$ becomes somewhat more complicated. This procedure is especially important at energies of order 100 MeV/nucleon, because at these energies σ_{nn} and σ_{np} differ by almost a factor of 3. Another effect manifested at low energies is due to the Coulomb interaction. The corresponding modification of the Glauber cross sections was made in Ref. 52.

Up to now we have discussed the factors whose inclusion does not take us beyond the optical limit. The solution of a number of problems related to the inclusion of various types of correlation (due to the Pauli principle, motion of the center of mass, interaction of the nucleons of the halo and the nucleons of the core), and also to the study of noneikonal terms, requires going beyond the optical limit of the Glauber approximation. All these problems are complicated and can be solved only approximately. The corrections for Pauli effects were studied in Ref. 58, where it was shown that they tend to decrease the cross sections by 5%. The factor describing the center-of-mass correlations for non-Gaussian densities in the Glauber calculations was determined in Ref. 59. The method of estimating the multiple integrals of the Glauber theory directly by the Monte Carlo method, proposed in Ref. 60, was used for this. It turned out that different approximations in the Glauber theory give differences in the differential cross sections of elastic scattering beyond the first diffraction maximum[59] and apparently weakly affect the total reaction cross sections. Correlations of the core and halo nucleons have been studied using the cluster approach to the Glauber theory in Ref. 61. It was shown that their inclusion tends to decrease σ_R and, accordingly, leads to larger values of the rms radii of the matter distribution $R_{\rm rms}$ when comparing theory and experiment. This fact induced the authors of Refs. 57 and 61 to review these quantities. For example, the value of $R_{\rm rms}$ increased by 14% and 7% for ^{11}Li and ^{11}Be, respectively.[57] On the other hand, in an analysis of the elastic scattering of ^{6}He and ^{8}He of energy 0.7 GeV/nucleon on protons,[62] no significant effect of cluster correlations on the extracted values of $R_{\rm rms}$ was found.

Let us summarize our discussion so far. At high energies ($E/A > 100$ MeV/nucleon) the optical limit in the approximation of zero interaction range is a fairly reasonable approximation of the Glauber theory for calculating the total reaction cross sections. The neglected factors (the finite interaction range and correlations) operate in different directions and cancel each other out in producing the value of σ_R. At low energies it is necessary to include correlations more accurately, especially when describing elastic scattering, along with noneikonal effects and Coulomb corrections.

2. THE EXPERIMENTAL DATA AND THEIR ANALYSIS

2.1. He isotopes

The measurement of the interaction cross sections σ_I for light exotic nuclei began with the study of helium isotopes. The cross sections σ_I for ^{3,4,6,8}He nuclei interacting with Be, C, and Al targets at 790 MeV/nucleon were first measured in Ref. 8. Measurements were later made for isotopes of Li, Be, and B.[9,10]

TABLE I. Rms radii (F) of proton, neutron, and matter distributions.

Nucleus	$R^G_{\rm rms}$	$R^P_{\rm rms}$	$R^N_{\rm rms}$	$R^M_{\rm rms}$	$R^C_{\rm rms}$
^{4}He	1.59±0.04	1.57±0.04	1.57±0.04	1.57±0.04	1.76±0.04
^{6}He	2.52±0.03	2.21±0.03	2.61±0.03	2.48±0.03	
^{8}He	2.55±0.03	2.15±0.02	2.64±0.03	2.52±0.03	
^{6}Li	2.35±0.03	2.32±0.03	2.32±0.03	2.32±0.03	2.46±0.02
^{7}Li	2.35±0.03	2.27±0.02	2.38±0.02	2.33±0.02	2.40±0.02
^{8}Li	2.38±0.02	2.26±0.02	2.44±0.02	2.37±0.02	
^{9}Li	2.32±0.02	2.18±0.02	2.39±0.02	2.32±0.02	
^{11}Li	3.10±0.17	2.88±0.11	3.21±0.17	3.12±0.16	
^{7}Be	2.33±0.02	2.36±0.02	2.25±0.02	2.31±0.02	
^{7}Be	2.38±0.01	2.34±0.01	2.40±0.01	2.38±0.01	2.47±0.01
^{10}Be	2.28±0.02	2.24±0.02	2.34±0.02	2.30±0.02	
^{11}Be	2.71±0.05	2.63±0.05	2.78±0.05	2.73±0.05	
^{12}Be	2.57±0.05	2.49±0.06	2.65±0.06	2.59±0.06	
^{14}Be	3.11±0.38	3.00±0.36	3.22±0.39	3.16±0.38	
^{8}B	2.39±0.04	2.45±0.05	2.27±0.04	2.38±0.04	
^{12}B	2.35±0.02	2.35±0.02	2.42±0.02	2.39±0.02	
^{13}B	2.42±0.11	2.41±0.11	2.50±0.12	2.46±0.12	
^{14}B	2.40±0.05	2.38±0.05	2.48±0.06	2.44±0.06	
^{15}B	2.40±0.25	2.37±0.26	2.49±0.28	2.45±0.27	
^{12}C	2.32±0.02	2.35±0.02	2.35±0.02	2.35±0.02	2.48±0.02

The simple parametrization of the cross sections (1) was used in Ref. 8, while in Ref. 9 the Glauber theory (Ref. 28; see also Ref. 63) was used for the first time to analyze the interaction cross sections of light exotic nuclei. In Table I we present the results of this analysis for a group of nuclei from Ref. 10. In the second column of the table we give the rms radii of the matter distribution for Gaussian density, and in columns 3–5 we give it for the harmonic-oscillator representation. In the last column are the charge radii obtained by folding of the proton distributions with the charge distribution in the proton ($r_p = 0.8$ F). Let us discuss the main regularities in the behavior of $R_{\rm rms}$ found in this analysis. For all isotope chains, $R_{\rm rms}$ is observed to grow significantly with increasing mass number, deviating from the $A^{1/3}$ dependence. In He isotopes this growth is observed in going from ^{4}He to ^{6}He and ^{8}He, in Li isotopes in going from ^{6}Li and ^{7}Li to ^{9}Li, and especially, ^{11}Li, and in Be isotopes in going to ^{11}Be and ^{14}Be, where $R_{\rm rms}$ for ^{11}Be is larger than for ^{12}Be. In boron isotopes, $R_{\rm rms}$ is observed to grow significantly in going from ^{14}B to ^{15}B. We note that $R_p > R_n$ for the two nuclei ^{7}B and ^{8}B, with the excess being quite large for ^{8}B. It follows from Table I that the observed regularities in the behavior of $R_{\rm rms}$ are independent of the representation used for the matter distribution density in the nuclei (Gaussian or harmonic oscillator). The data indicate that the radii have a strong isotopic dependence. It was shown in Ref. 10 that comparison with the Hartree–Fock calculations[64] confirms the importance of including the density dependence of the effective forces used in that method for explaining the observed behavior of the radii in moving along isotope chains.

The Glauber approximation based on the cluster approach to the structure of light exotic nuclei was used in Ref. 57 to analyze the interaction cross sections in order to extract

TABLE II. Rms radii of matter distributions calculated in the Glauber approximation.

Nucleus	Rms radius (F)	σ_I (exp., mb)	Reference	Method
^{4}He	1.58±0.04	503±5	8	SD
^{6}He	2.71±0.04	722±5	8	FB (a)
	2.69±0.04			FB (b)
^{7}Be	2.31±0.05	738±9	9	SD[61]
^{8}B	2.50±0.04	798±6	20	FB[61]
^{9}Li	2.30±0.02	796±6	9	SD
^{11}Li	3.53±0.10	1060±10	65	FB (a)
^{10}Be	2.28±0.02	813±10	9	SD
^{11}Be	2.90±0.05	942±8	10	FB (a)
^{12}Be	2.54±0.05	927±18	10	SD
^{14}Be	3.20±0.30	1109±69	66	FB (a)

$R_{\rm rms}$. The authors of that study performed two variants of the calculations, neglecting correlations between nucleons from the clusters making up the incident particle [the static-density (SD) approximation] and including these correlations [the few-body (FB) approximation]. The results of the analysis are shown in Table II along with the experimental values of σ_I at energy 790 MeV/nucleon. For ^{12}C target nucleus, in all cases the Gaussian representation with $R_{\rm rms}=2.32$ F (Ref. 10) was used, and $\bar{\sigma}_{NN}$ was taken to be the cross section for free NN scattering, parametrized in Ref. 52. Two slightly different cluster descriptions were used for ^{6}He and led to practically the same result for $R_{\rm rms}$. The difference was less than 1%. The results shown in Table II confirm the general regularities in the behavior of $R_{\rm rms}$ found in Ref. 10.

The authors of Ref. 57 pointed out the need to go beyond the optical limit, i.e., the SD approximation, in constructing the total reaction cross sections for light exotic nuclei. The simple binary cluster model[67] has been used to calculate σ_R as a function of the projectile radius. These results are shown in Fig. 1. It can be seen that the cross sections in the FB approximation are smaller than the corresponding σ_R obtained in the SD approximation. This difference in the cross sections grows with increasing $R_{\rm rms}$ from 2% at $R_{\rm rms}=2.4$ F to 8% at $R_{\rm rms}=3.1$ F. Although these differences are small, the accuracy in measuring σ_I reaches 1–2% (see Table II), and so reliable extraction of the radii from the measured cross sections σ_I requires calculations of a corresponding accuracy.

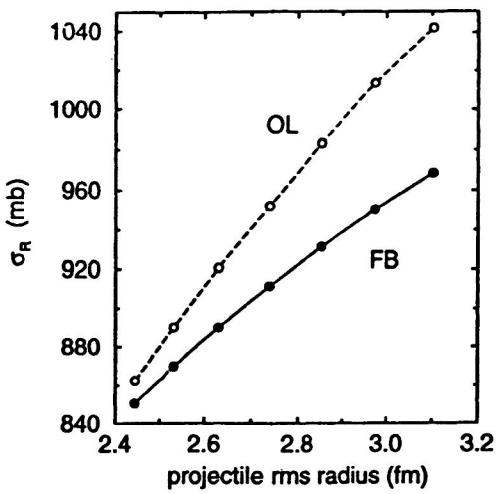

FIG. 1. Total reaction cross sections σ_R, calculated in the optical limit (OL) and the few-body approximation (FB) of the Glauber theory.

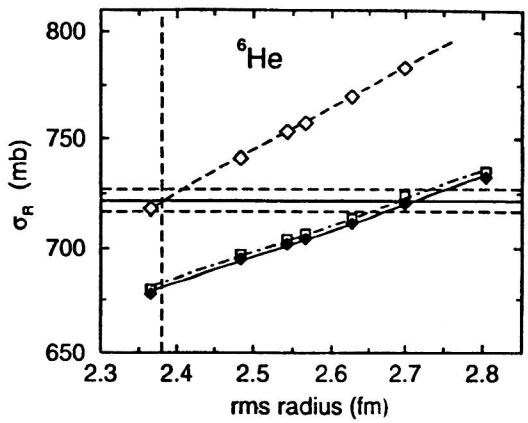

FIG. 2. Total reaction cross sections σ_R, calculated for ^{6}He at energy 800 MeV/nucleon in the Glauber approximation.

The decrease of the cross section in the calculations including correlations between the nucleons in clusters leads to an increase in the nuclear radii extracted from comparison of theory and experiment. The authors of Ref. 57 therefore reviewed the results of their earlier analysis for a number of light exotic nuclei. The corresponding results for ^{6}He at 800 MeV/nucleon are shown in Fig. 2. The cross sections calculated in the SD approximation are shown by the squares along the dashed line, and those for the FB approximation are shown by the squares along the solid line. The squares along the dot–dash line correspond to a different method of describing the cluster structure of ^{6}He. The horizontal lines determine the error corridor for the values of σ_I measured experimentally. We see that the inclusion of correlations between nucleons in clusters tends to increase the ^{6}He radius from 2.38 F to 2.71 F.

As is well known, in going from high to lower energies ($E/A<100$ MeV/nucleon), i.e., to intermediate energies, the cross sections for nucleon–nucleon scattering grow, while the reaction cross sections become more sensitive to the matter distribution in the peripheral region of the projectile particles.[17] In addition, nuclear and Coulomb effects are more easily distinguished at intermediate energies.[65]

The total reaction cross sections σ_R for a large group of light exotic nuclei at intermediate energies were first measured in Ref. 13. A silicon target and a new, direct, method of obtaining the cross sections were used. The experiments were performed for projectile energies ranging from 20 to 50 MeV/nucleon. The strong-absorption model with the Kox parametrization (2) was used to analyze the experimental data. On the whole, the results obtained at intermediate energies confirmed the regularities observed in analyzing the experimental data on σ_I at high energies.[8–10] The value $r_0=1.33$ F was obtained for ^{8}He (Ref. 13). This is considerably larger than the standard value $r_0\approx 1.10$ F used to describe the interaction of stable nuclei.

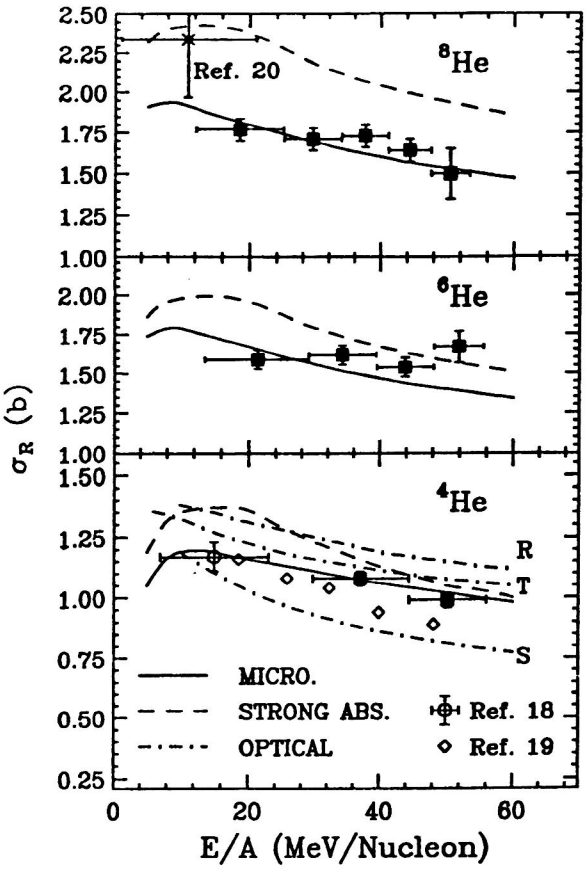

FIG. 3. Total reaction cross sections σ_R, measured at the corresponding energy for ^{4,6,8}He nuclei interacting with ^{28}Si, together with the theoretical predictions and the data of other laboratories.

Other measurements of σ_R at intermediate energies were performed in Refs. 16 and 17. The experimental data for ^{4,6,8}He interacting with ^{28}Si in the energy range from 20 to 60 MeV/nucleon are given in Fig. 3 along with the theoretical predictions and the data from other laboratories.[13,68,69] The optical limit of the Glauber approximation[53,70,71] was used in Ref. 16 as the microscopic approach. The symbols R, T, and S in Fig. 3 refer to the choice of optical-model parameters from Refs. 72–74, respectively. We see that on the whole, the Glauber approximation gives a good description of the experimental data. However, for ^{6}He the theoretically predicted falloff of the cross sections with increasing energy is not observed experimentally. Moreover, the experimental value of σ_R for ^{8}He from Ref. 13 lies considerably higher than the predictions of the Glauber calculations. The strong-absorption model gives a poorer description of the experimental values of σ_R for all three helium isotopes, especially ^{8}He. The optical-model calculations for ^{4}He give a satisfactory description of σ_R only when the set of parameters from Ref. 73 is used.

2.2. Li isotopes

The series of lithium isotopes contains the ^{11}Li nucleus, which possesses perhaps the most exotic properties of any of the light exotic nuclei: it has a very small separation energy of the last two neutrons, a very extended halo, and significant differences in the proton and neutron distributions. The first measurements of σ_I at 790 MeV/nucleon for Li isotopes were made in Ref. 9. The experimental data were analyzed in the Glauber approximation. The results were discussed in the preceding section (Table I).

TABLE III. Strong-absorption radii for Li isotopes, extracted from analysis of $\sigma_R(\sigma_I)$ measured at various energies.

	E/A, MeV/nucleon		
Nucleus	30	80	790
^{8}Li	1.282±0.010	1.177±0.037	1.167±0.010
^{9}Li	1.227±0.010	1.058±0.017	1.151±0.007
^{11}Li	1.222±0.029	1.429±0.047	1.300±0.0053

A complex experimental analysis of ^{9}Li and ^{11}Li was performed in Ref. 11. The interaction cross sections σ_I were measured on proton and deuterium targets, and also on Be and C, at 400 and 800 MeV/nucleon; the transverse-momentum distributions of ^{9}Li and neutrons in the fragmentation of ^{11}Li were extracted; and the momentum correlations of the neutrons in the halo were studied. The analysis was performed using two variants of the Glauber approximation: the halo neutrons were assumed to be either in the $1p$ or in the $2s$ orbital. The rms matter radius $R_{\rm rms}(^{11}\text{Li})$ was found to be 3.12±0.30 F in the case of the $1p$ orbital and 3.05 ±0.30 F in the case of the $2s$ orbital. Therefore, different assumptions about the nature of the single-particle motion of the halo neutrons affect the value of $R_{\rm rms}(^{11}\text{Li})$ extracted from analysis of σ_I only at the 2% level. The matter density in ^{11}Li was chosen to have the form

$$\rho(^{11}\text{Li})=\rho_{\rm core}+\rho_{\rm halo}, \tag{22}$$

where the ^{9}Li nucleus was treated as the core. In this analysis it was found that $R_{\rm rms}(^9\text{Li})=2.61\pm0.10$ and 2.50 ± 0.10 F, respectively, while in both cases $R_{\rm rms}(\text{halo})=4.8\pm0.8$ F. Analysis of σ_I and also the momentum distributions and correlations in the neutron momenta led the authors[11] to conclude that a neutron halo exists in ^{11}Li.

The total reaction cross sections σ_R for ^{9}Li and ^{11}Li were measured on a silicon target at energies of 31.584 and 25.507 MeV/nucleon, respectively, in Ref. 13. Analysis of the experimental data using the strong-absorption model with the Kox parametrization led to values of the radius parameter $r_0=1.168$ F for ^{9}Li and $r_0=1.42$ F for ^{11}Li, which slightly exceeds the standard value $r_0=1.1$ F for ^{9}Li and is much larger than the value $r_0=1.33$ F for ^{8}He.

Other measurements at intermediate energies were performed in Ref. 14. In Table III we present the results of the analysis[14] at 80 MeV/nucleon, along with ones at 30 MeV/nucleon (Ref. 75) and at 790 MeV/nucleon (Ref. 9). It should be noted that these results suggest the value 1.222 F for ^{11}Li at $E/A=30$ MeV/nucleon, while otherwise they are consistent with the known regularities: the significant increase of the strong-absorption radius for ^{11}Li compared to ^{8,9}Li, while the increase at 30 MeV/nucleon for ^{8}Li and ^{9}Li reflects the increase of the nucleon–nucleon cross sections with decreasing energy. The authors of Ref. 15 note that the measurements at 80 MeV/nucleon are supplemented by the earlier

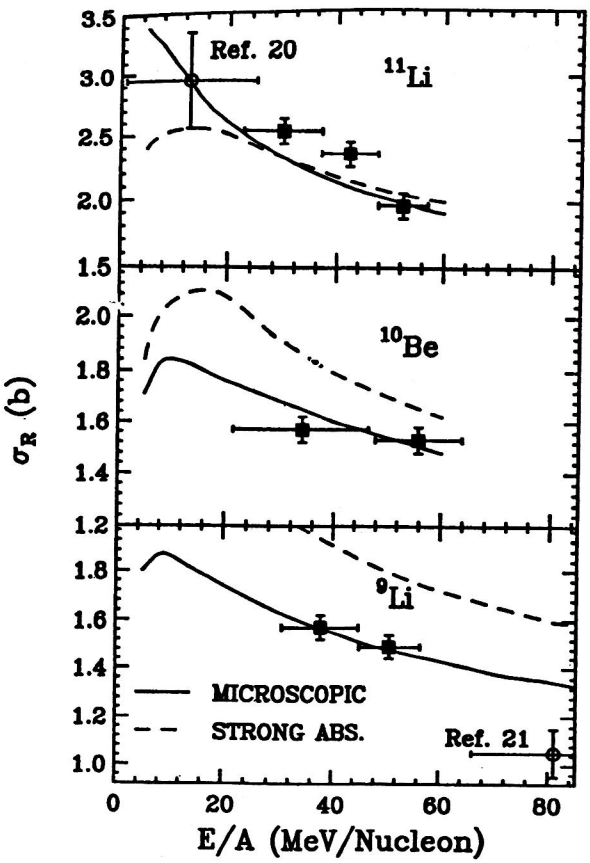

FIG. 4. The same as in Fig. 3, for ^{9,11}Li and ^{10}Be.

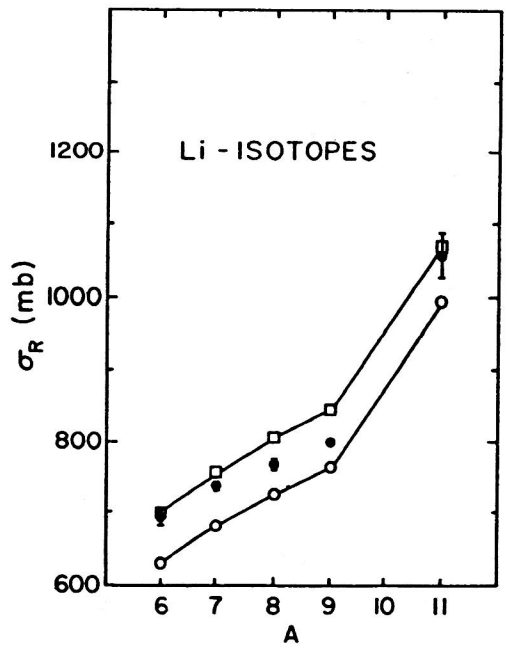

FIG. 5. Total reaction cross sections σ_R, calculated in the Glauber approximations for Li isotopes.

measurements at 790 and 30 MeV/nucleon, and confirm the conclusion that only a matter distribution with a long neutron tail for ^{11}Li, which, according to the quantum-mechanical description, is due to the very small binding energy of the last two neutrons, corresponds to an adequate description of the experimental data.

As mentioned in the preceding section, the measurements of Ref. 16 were performed in the energy range from 20 to 60 MeV/nucleon. In Fig. 4 we show the results for ^{9,11}Li and ^{10}Be along with the theoretical calculations and data from other laboratories. We see that, on the whole, the Glauber approximation (referred to by the authors as the microscopic approach) gives a satisfactory description of the experimental data. However, there is a significant discrepancy for the value of σ_R obtained at 80 GeV/nucleon for ^{9}Li. The strong-absorption model gives a poorer description of the experimental cross sections.

In addition to the studies mentioned above, there have been several others devoted to the analysis of $\sigma_I(\sigma_R)$ for Li isotopes. In Ref. 53 the Glauber approximations with zero and finite interaction range [Eqs. (17) and (20), respectively] were used to calculate σ_I at 800 MeV/nucleon for Li and Be isotopes. The nucleon–nucleon cross section $\bar{\sigma}_{NN}$ was taken to be 40 mb, and the value 1.0 F was used for the interaction range. The calculated σ_R together with the experimental data are shown in Fig. 5. Here the squares correspond to finite interaction range, the circles to zero range, and the black points to the experimental data. We see that for ^{6,7}Li and ^{11}Li fairly good agreement with experiment is obtained in the finite-range approximation, while for ^{8}Li and ^{9}Li the experimental points lie between the theoretical values from the two variants. In any case, the disagreement between theory and experiment amounts to a few percent. Several methodological calculations are also presented in Ref. 53. It is shown that when $\bar{\sigma}_{NN}$ is decreased by 20%, the reaction cross section σ_R falls by 7%, while a 20% decrease of the interaction range causes σ_R to fall by only 2.5%. The Hartree–Fock method with the SGII interaction[76] was used to construct the ^{11}Li density, and an orbital-dependent renormalization coefficient was introduced for the one-particle SGII potential. This factor was chosen so as to obtain the experimental value of the neutron separation energy. As a result, the value $R_{\rm rms}=2.846$ F was obtained for ^{11}Li, which is 8% smaller than in Ref. 11.

The cluster approach in the Glauber approximation has been used[57] to analyze σ_R for ^{11}Li at 800 MeV/nucleon. The analysis scheme is the same as for ^{6}He (see the preceding section). The results are given in Fig. 6. We see that, as in the case of ^{6}He, $R_{\rm rms}(^{11}{\rm Li})$ is significantly increased when correlations between nucleons in the clusters forming ^{11}Li are included. The new value found for the rms radius was $R_{\rm rms}=3.53\pm0.10$ F, which is 14% larger than the earlier value obtained in Ref. 57. Another result obtained in Ref. 57 follows from analysis of the effect of the choice of cross section σ_{NN} on the calculation of σ_R. In Fig. 7 we show two calculations of σ_R for the ^{11}Li+^{12}C system together with two experimental points. The solid line corresponds to the calculation using σ_{NN} taken from Ref. 52, and the dashed line to σ_{NN} from the systematics in Ref. 55. Unfortunately, experimental data are available only for two values of the energy, and for these two values the theoretical results are nearly the same. The two calculational variants give similar results at energies above 300 MeV/nucleon, while at intermediate energies ($\sim$100 MeV/nucleon) the discrepancies reach 8%.

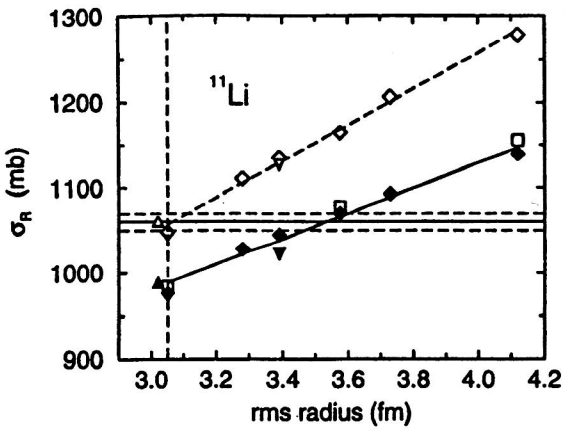

FIG. 6. The same as in Fig. 2, for ^{11}Li.

The analysis of σ_R at energies below 100 MeV/nucleon should be performed using optical-model calculations. Regarding the cluster approach, we note that already in Ref. 77 the cluster model was used to show that calculations in the optical limit of the Glauber theory overestimate σ_R, the error being larger, the smaller the projectile energy.

A semi-microscopic approach with density functional was developed in Refs. 39 and 78 for describing the interaction of light exotic nuclei with stable nuclei. Its main features are the following: (1) the neutron and proton densities for all nuclei, both projectiles and targets, are calculated with a single set of fixed parameters, using the density-functional method,[31] where no additional conditions such as the requirement that the experimental values of the nucleon separation energies be reproduced are introduced into the calculation; (2) at low and intermediate energies ($E/A<100$ MeV/nucleon) the total reaction cross sections σ_R are calculated in the semi-microscopic optical model using double-folding potentials with the explicit inclusion of one-nucleon exchange effects in the real part of the optical potential. The imaginary part is made up from the real part in accordance with Eq. (14); (3) at high energies ($E/A>100$ MeV/nucleon) σ_R is calculated in the optical limit of the Glauber theory. This approach has been used[79] to analyze the potentials for neutron-rich Li isotopes interacting

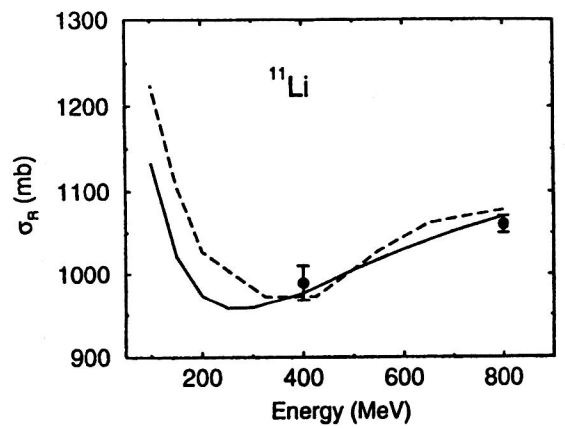

FIG. 7. Experimental (points) and calculated (in the Glauber approximation) total reaction cross sections σ_R for ^{11}Li interacting with ^{12}C.

TABLE IV. Total reaction cross sections σ_R (mb), calculated in the Glauber approximation with the densities of the density-functional method.

System	E/A (MeV/nucleon)	σ_R, theor.	σ_I, exp.
^{8}B+^{12}C	800	838	798±6[20]
^{11}Li+^{12}C	400	959	989±21[11]
^{11}Li+^{12}C	800	1050	1056±14[11]

with stable nuclei. In Refs. 39 and 80 the semi-microscopic approach with density functional was used to obtain a reasonable description of the quasielastic scattering of light exotic nuclei at intermediate energies. Isobar scattering on a target nucleus with $N\neq Z$ was analyzed in Ref. 81. In Refs. 82 and 83 the semi-microscopic approach with density functional was used to analyze the energy dependence of σ_R, and in Ref. 84 to describe the experimental σ_I for nuclear isobars with $A=20$ at energy 950 MeV/nucleon. Some of the results of those studies will be discussed in this and the following sections.

In Table IV we give the σ_R calculated in the semi-microscopic approach with density functional at high energies.[84] We see that the agreement between theory and experiment is fairly good. In Fig. 8 we show the calculated (lines) and experimental (points) values of σ_R for the ^{11}Li+^{12}C system. The calculations were performed using the semi-microscopic approach with density functional and double-folding potentials.[82] As noted earlier in this review, when the optical model is used an arbitrariness associated with the choice of parameters of the absorption potential arises. This arbitrariness can be eliminated if the measured angular distributions of (quasi)elastic scattering and the total reaction cross sections σ_R are available at the same energy. Unfortunately, for ^{11}Li+^{12}C the angular distributions have been measured only at 60 MeV/nucleon,[38] and σ_R at other energies. The curves for $\sigma_R(E)$ in Fig. 8 were calculated for three sets of absorption parameters. Here $N_w=0.3$ and the values of α_w are given in the figure. The points correspond to

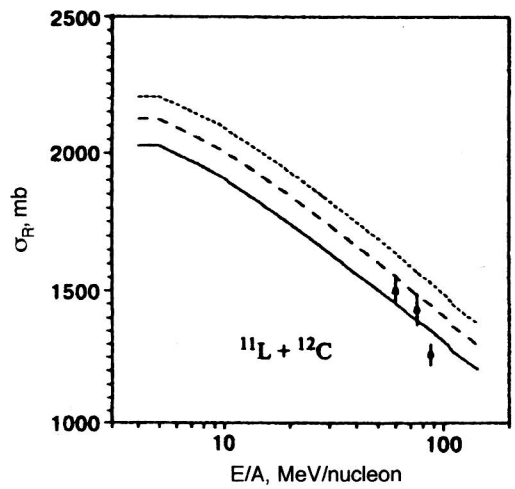

FIG. 8. Experimental (points) and calculated (in the double-folding model) total reaction cross sections σ_R for ^{11}Li interacting with ^{12}C. The solid curve is for $\alpha=0.02$, the dashed curve is for $\alpha=0.035$, and the dotted curve is for $\alpha=0.05$.

the experimental data from Refs. 15 and 85. We see that σ_R depends strongly on energy, falling off at lower energies (not shown in the figure). Good agreement with the experimental data is obtained for reasonable values of the absorption parameters.

The neutron and proton densities enter separately into computational schemes using the semi-microscopic approach with density functional, both in the optical limit of the Glauber theory and in the double-folding model. All the calculations for ^{11}Li were performed with densities constructed by the density-functional method, with rms radii $R_{\rm rms}(n) = 3.255$ F, $R_{\rm rms}(p) = 2.235$ F, and $R_{\rm rms}(m) = 3.011$ F (Ref. 39). This result for $R_{\rm rms}(m)$ differs by only 3% from that obtained for ^{11}Li (Ref. 11) by analyzing high-energy experiments. It follows from these values of the radii that in the semi-microscopic approach with density functional, $\Delta r_{np} = R_{\rm rms}(n) - R_{\rm rms}(p) = 1.20$ F. Therefore, the analysis performed in the semi-microscopic approach with density functional confirms the hypothesis that a neutron halo exists in ^{11}Li.

Double-folding potentials were also used in Refs. 35, 40, and 41 to calculate σ_R for ^{11}Li. The calculation for the ^{11}Li+^{28}Si system at energy 29 MeV/nucleon with potential parameters extracted from a description of elastic scattering did not result in agreement with the experimental data[13] at 25.5 MeV/nucleon. The angular distributions and σ_R were analyzed simultaneously for the ^{11}Li+^{12}C system at 60 MeV/nucleon in Ref. 40. The value $\sigma_R = 1473$ mb, close to that found from the systematics in Ref. 38, was obtained when the absorption-potential range was increased by 10% and polarization terms were included at the phenomenological level in the real and imaginary parts of the optical potential. Theory and experiment for σ_R are also compared in Ref. 40 for two values of the energy, 75 and 87 MeV/nucleon. However, the angular distributions of the quasielastic scattering of ^{11}Li on ^{12}C at these energies have not yet been measured. Yet another combined analysis of the angular distributions and σ_R for the ^{11}Li+^{12}C system was performed in Ref. 41. That analysis used double-folding potentials constructed with the JLM interaction.[50] Inclusion of the renormalization factors λ_R and λ_I for the real and imaginary parts of the optical potential allowed the experimental data to be described at the former level.[38–40] The calculations performed in the same study[41] in the Glauber approximation gave values of σ_R lying below the experimental points and the values obtained in the folding model.

2.3. Be and B isotopes

Among light nuclei, the Be and B isotope chains are distinguished by the fact that at their ends are nuclei with opposite types of proton and neutron distributions: for Be isotopes, ^{7}Be has $R_{\rm rms}(p) > R_{\rm rms}(n)$, while ^{11}Be and ^{14}Be have the clearly expressed properties of a neutron halo. For B isotopes, ^{8}B is the first candidate for a nucleus with a proton halo, while ^{15}B, ^{17}B, and ^{19}B show signs of a neutron halo.

The interaction cross sections for Be and B isotopes were first measured at 790 MeV/nucleon in Refs. 9 and 10.

TABLE V. Total reaction cross sections σ_R (b) and interaction cross sections σ_I (b) for ^{11}Be, experiment and theory.

	$E/A = 33$ MeV/nucleon			$E/A = 790$ MeV/nucleon		
System	exp.	Glauber	Kox	exp.	Glauber	Kox
^{11}Be+^{12}C	1.56±0.03	1.60	1.30	0.942±0.008	1.02	0.839
^{11}Be+^{27}Al	2.27±0.05	2.25	1.76	1.38±0.03	1.46	1.227

The results are given in Table I and were discussed in Sec. 2.1 of the present review. The cross sections σ_R for ^{11}Be interacting with ^{12}C and ^{27}Al targets at 33 MeV/nucleon were obtained in Ref. 86. The corresponding data and the results of their analysis are given in Table V, along with the data[10] at 790 MeV/nucleon. We see that the Glauber calculations give a good reproduction of σ_R at intermediate energies and σ_I at high energies, while the Kox parametrization underestimates the cross sections compared to experiment. Analysis of the matter distribution in ^{11}Be led the authors of Ref. 86 to conclude that ^{11}Be, like ^{11}Li, has a neutron halo. In Ref. 10, using two variants for ^{11}Be, the values $R_{\rm rms} = 2.71 \pm 0.05$ F and 2.52 ± 0.03 F were found, while the analysis of Ref. 53 gave the values 2.772 and 2.722 F. A calculation using the semi-microscopic approach with density functional[81] gave $R_{\rm rms} = 2.517$ F for ^{11}Be, with $\Delta r_{np} = 0.411$ F. Finally, in a review of the values of $R_{\rm rms}$ in connection with including correlations between nucleons in clusters, the larger value $R_{\rm rms}(^{11}{\rm Be}) = 2.90 \pm 0.05$ F was obtained.[57]

In Ref. 13, σ_R was measured for a large group of nuclei, including B isotopes, at intermediate energies. For ^{15}B the value $r_0 = 1.284$ F was obtained using the strong-absorption model. This is considerably larger than the standard value $r_0 = 1.1$ F. A large group of light exotic nuclei, including the new mirror pairs ^{9}C–^{9}Li, ^{10}C–^{10}Be, and ^{13}O–^{13}B was studied in Ref. 19. In particular, the interaction cross sections σ_I were measured at an energy greater than 730 MeV/nucleon for ^{15}B. The results are given in Table VI. We see that the cross sections σ_I grow with increasing mass number of the target nucleus, and increase slightly with increasing energy for a ^{12}C target. Analysis using the Glauber approximation led the authors of Ref. 19 to the conclusion that ^{15}B is a candidate for a nucleus with a neutron halo. Recently, σ_I has been measured at 740 MeV/nucleon for ^{14}Be and ^{17,19}B interacting with a ^{12}C target.[87] The analysis was carried out using the Glauber approximation. The authors confirm the conclusion that the nuclear radii are larger, the smaller the nucleon separation energy. They also conclude that ^{17,19}B

TABLE VI. Interaction cross sections σ_I (mb) measured for ^{15}B.

Target nucleus	E/A (MeV/nucleon)	σ_I (mb)
Be	770	931±17
C	760	1000±20
C	740	965±15
Al	760	1384±30

TABLE VII. Total reaction cross sections σ_R (mb) for ^{7}Be and ^{8}B, calculated in various approaches.

	^{7}Be+^{12}C	^{8}B+^{12}C
JLM[a]	1026	1104
Kox[b]	1037	1186
Kox[c]	1062	1179
Glauber[d]	1034	1111
Glauber[e]	1080	1130
Exp.[f]	738±9	784±14

[a]Folding model with JLM interaction and shell-model densities.
[b]Kox parametrization with modification from Ref. 36.
[c]Kox parametrization with shell-model radii.
[d]Glauber approximation with densities of the Hartree-Fock method.
[e]Glauber approximation with shell-model densities.
[f]Ref. 10.

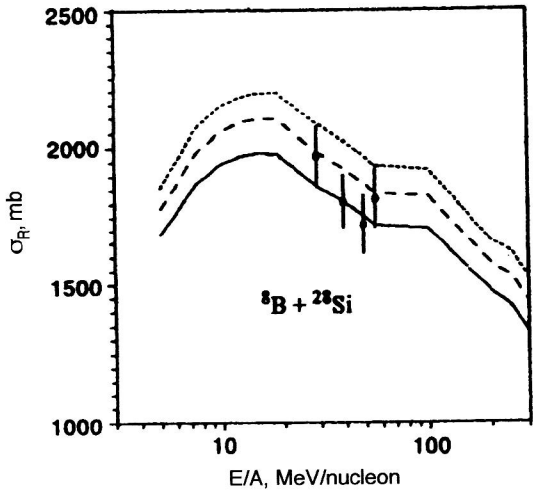

FIG. 9. Energy dependence of the total reaction cross sections σ_R for the ^{8}B+^{28}Si system. The solid curve is for α=0.03, the dashed curve is for α=0.06, and the dotted curve is for α=0.09; the points are experimental data.

have a neutron cloud and discuss the structure of the possible neutron halo in ^{14}Be and ^{19}B.

Calculations using the Glauber approximation with zero and finite interaction range have been performed for Be isotopes at 790 MeV/nucleon in Ref. 53. As in the case of Li isotopes (see Fig. 5 in the present review), for lighter isotopes (^{10,11,12}Be) the approximation with zero interaction range reproduces the experimental values of σ_I better, while the approximation with finite interaction range works better for ^{14}Be. The angular distributions of the elastic scattering of ^{12}Be and ^{14}Be on ^{12}C at 56 MeV/nucleon were measured in Ref. 36, and in analyzing these data the values of σ_R were calculated using the macroscopic optical model. The values 1238 and 1900 mb were obtained for ^{12}Be and ^{14}Be, respectively. These results are consistent with the experimental data at high energies. Considerably smaller values, 911 and 1123 mb, respectively, were obtained in a review of the optical-model analysis of these data in Ref. 37. In concluding our review of the situation regarding the more massive Be isotopes, we note that a good description of σ_R for ^{10}Be at intermediate energies (see Fig. 4) has been obtained[16] in the Glauber approximation, while the strong-absorption model underestimates the values of σ_R compared to experiment.

Many studies have been devoted to the lightest Be and B isotopes, namely, the ^{7}Be and ^{8}B nuclei, in order to determine the dimensions of their proton cloud. Other properties of these nuclei have also been studied. As noted above, the first measurements of σ_I for ^{7}Be and ^{8}B at high energies were made in Refs. 9 and 10. The analysis gave $R_{\rm rms}$=2.39 ±0.04 F for ^{8}B. The electric quadrupole moment of ^{8}B was measured in Ref. 12 and turned out to be considerably larger than predicted by the shell-model calculations. It was therefore concluded that ^{8}B is the first candidate for a nucleus with a proton halo.

The angular distributions of the quasielastic scattering of ^{7}Be and ^{8}B at 40 MeV/nucleon on a ^{12}C target were measured in Ref. 88. As a part of a semi-microscopic analysis of the experimental data, the densities were constructed by the Hartree–Fock method, and the values $R_{\rm rms}(m)$=0.075 and 2.207 F were obtained for ^{7}Be and ^{8}B, respectively.[88] The values of σ_R calculated in different variants at energy 40 MeV/nucleon[88] are shown in Table VII along with the experimental data at high energies. It can be seen that the theoretical cross sections σ_R are close to each other and significantly larger than the experimental cross sections σ_I at high energy. The latter reflects the fact that at intermediate energies the *NN*-scattering cross section is larger than at high energies.

The experimental data from Ref. 88 were analyzed using the semi-microscopic approach with density functional in Ref. 39. A reasonable description of the angular distributions was obtained when using the densities of the density-functional method, and the calculated rms matter radii $R_{\rm rms}$ for ^{7}Be and ^{8}B turned out to be 2.420 and 2.507 F, respectively, i.e., significantly larger than in Ref. 88. The size of the proton cloud was found to be 0.49 F for ^{8}B and 0.312 F for ^{7}Be. The cross sections σ_R calculated in Ref. 39 with the absorption parameters determined from the description of elastic scattering turned out to be 1102 mb for ^{7}Be and 1201 mb for ^{8}B, which is quite close to the results in Table VII.

The values of σ_R for ^{8}B nuclei interacting with a ^{28}Si target were measured in the energy range from 20 to 60 MeV/nucleon in Ref. 17. It was possible to obtain a good description of the data in the Glauber approximation by using the densities from Ref. 12, for which $R_{\rm rms}(m)$=2.72 F and Δr_{np}=−0.78 F, i.e., for geometrical parameters even larger than those found in Ref. 39. In Fig. 9 we show the values of σ_R calculated using the semi-microscopic approach with density functional[82] for the ^{8}B+^{28}Si system along with the experimental data from Ref. 11. The angular distributions of the elastic scattering of ^{8}B on ^{28}Si have not yet been measured, and so several sets of absorption parameters were used in the calculations of Ref. 82. We see that there is good agreement between theory and experiment for reasonable values of the absorption-potential parameters.

New experimental data on ^{7}Be and ^{8}B were obtained in Ref. 18, and as a part of their analysis the ideas of Ref. 88 about the size of the proton cloud in ^{8}B were reviewed. The cross sections σ_R were measured in Ref. 18 for ^{7}Be and ^{8}B on a ^{28}Si target in the energy range from 10 to 40 MeV/nucleon. The results are given in Table VIII. The values of

TABLE VIII. Total reaction cross sections σ_R (b) for ^{7}Be and ^{8}B interacting with a ^{12}C target nucleus at intermediate energies.

^{7}Be		^{8}B	
E/A, MeV/nucleon	σ_R (mb)	E/A, MeV/nucleon	σ_R (mb)
38.46±0.56	1491±84	37.96±0.76	1642±75
36.48±0.58	1476±56	35.23±0.82	1698±70
31.80±2.15	1597±56	28.34±3.23	1861±67
23.46±2.76	1603±48	15.28±4.88	1940±97

σ_R decrease with increasing energy for both projectiles, and for ^{8}B the specific change of σ_R, i.e., the change per unit energy range, is larger, because the measurements for ^{8}B pertain to the energy range in which the reaction cross sections σ_R are most sensitive. The values of σ_R measured for ^{8}B are smaller at the corresponding energies than those measured in Ref. 17. The distribution radii used in Ref. 18, along with the data of other studies, are given in Table IX, taken from Ref. 18. Now the values of $R_{\rm rms}(m)$ for ^{8}B are considerably larger than in Ref. 88, and the value 0.487 F for the proton cloud is very close (a difference of less than 1%) to the value 0.49 F predicted earlier in Ref. 39.

The energy dependence of σ_R for ^{7}Be and ^{8}B, along with the results of the Glauber and optical-model calculations, is shown in Fig. 10, taken from Ref. 18. Here the light (dark) circles are the experimental σ_R for ^{7}Be (^{8}B). We see that for ^{8}B at lower energies the semi-microscopic optical model gives a better description of σ_R, whereas for ^{7}Be the predictions of the optical model and the Glauber approximation with finite interaction range are roughly the same in this energy range. In Fig. 11, also taken from Ref. 18, we show all the results for ^{7}Be and ^{8}B, including the data on the breakup reaction, and also the cross sections σ_R for ^{8}B+^{28}Si, measured in Ref. 17 (dark triangles), and the cross sections σ_I for ^{7}Be and ^{8}B interacting with Al at high energies, measured in Ref. 10 (stars).

The cross sections σ_R have recently been measured for ^{8}B interacting with Be, C, and Al targets at energies of about 40 and 60 MeV/nucleon.[89] These data are given in Table X along with the results of the calculations using the semi-microscopic approach with density functional.[84] We see that there is good agreement between theory and experiment, although the experimental σ_R have a stronger energy dependence. This apparently is an indication of the importance of including the energy dependence of the absorption-potential parameters.

TABLE IX. Rms radii (F) of the proton, neutron, and matter distributions for ^{7}Be, ^{8}B, and ^{28}Si.

Nucleus	r_p	r_n	r_m	$r_p - r_n$	Model
^{7}Be	2.369	2.155	2.280	0.214	HF Skll
^{8}B	2.754	2.267	2.582	0.487	HF Skll+SM
	2.759	2.155	2.549	0.604	HF Skll
	2.790	2.247	2.600	0.543	WS, β=0.6
	2.74	2.25	2.57	0.49	RGM[10]
	2.88	2.47	2.73	0.41	GCM[11]
^{28}Si	3.061	3.025	3.043		HF Skll

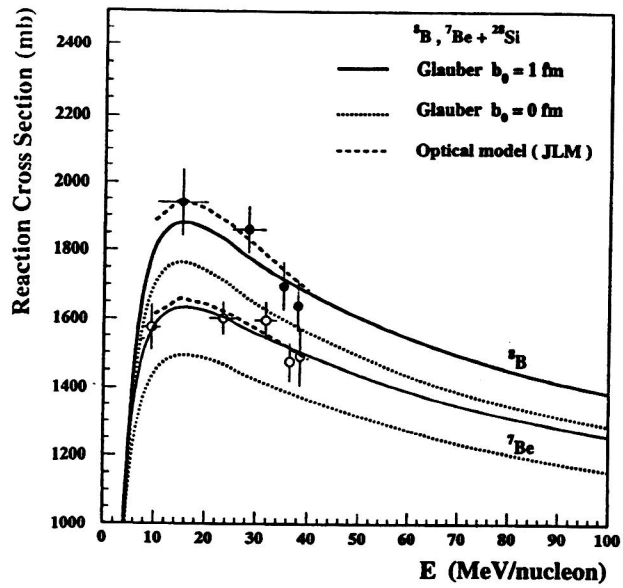

FIG. 10. Energy dependence of the total reaction cross sections σ_R for ^{7}Be and ^{8}B, compared with the Glauber and optical-model calculations.

The total interaction cross sections for ^{7}Be, ^{8}B, and ^{9}C, the cross sections for stripping a proton from ^{8}B and ^{9}C, and also the cross sections for stripping two protons from ^{9}C were measured in Ref. 90, using targets ranging from carbon to lead at energy 285 MeV/nucleon. Additional measurements were also performed for ^{8}B at 142 MeV/nucleon. The analysis using the Glauber approximation of both the data obtained by the authors and also the data from other studies led to the conclusion[90] that the full set of experimental results for ^{8}B can be explained only by assuming that ^{8}B is a nucleus with a clearly expressed proton halo of size apparently smaller than that of the halo in neutron-rich nuclei, while the use of the standard densities allows a description of the data for ^{7}Be and ^{9}C within the error.

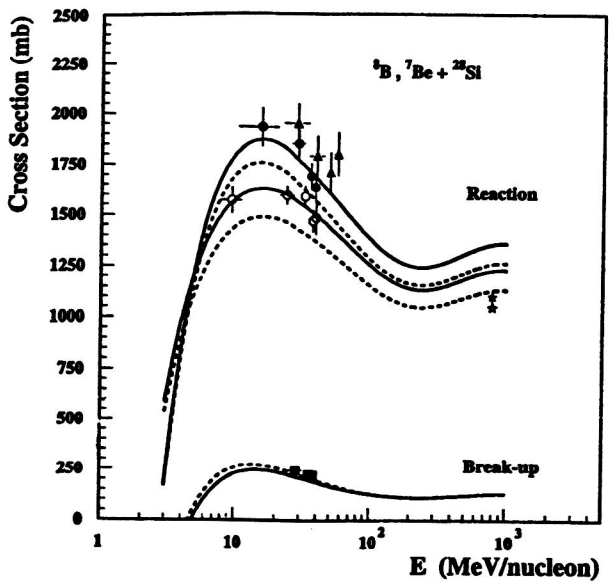

FIG. 11. Total reaction cross sections and breakup cross sections for the ^{8}B+^{28}Si and ^{7}Be+^{28}Si systems.

TABLE X. Total reaction cross sections σ_R (mb) for ^{8}B, calculated in the double-folding model and the experimental data.

Nucleus	E/A (MeV/nucleon)	N_w	α	σ_R	σ_R (exp.)
^{9}Be	40	0.5	0.02	1173	1306(13)
^{9}Be	60	0.5	0.02	1058	1087(24)
^{12}C	40	0.3	0.03	1200	1274(12)
^{12}C	60	0.3	0.03	1080	1103(18)
^{27}Al	40	0.3	0.045	1730	1803(21)
^{27}Al	60	0.3	0.03	1530	1621(35)

A repeat measurement of σ_I for ^{8}B on a ^{12}C target at 790 MeV/nucleon was performed in Ref. 20. It led to a slight improvement of the earlier value of σ_I obtained in Ref. 9, and the experimental error was reduced. This value is given in Table IV of the present review. We see that the theoretical calculation using the semi-microscopic approach with density functional[84] reproduces the experimental values of σ_I well. To conclude this subsection, we note that in the cluster approach realized within the Glauber approximation,[61] the value $R_{\rm rms}(m)=2.50\pm0.04$ F is obtained for ^{8}B, which is close to the corresponding values discussed above.

2.4. Na isotopes

The total reaction cross sections σ_R for heavy Na isotopes have been measured at 40–50 MeV/nucleon in Ref. 13. Analysis of the experimental data using the strong-absorption model led to the discovery of a significant isotopic dependence of the strong-absorption radius, from 1.035 F for ^{26}Na to 1.159 F for ^{30}Na.

Measurements of σ_I at 950 MeV/nucleon on a carbon target were performed for a large group of Na isotopes with mass numbers $A=20-23$ and 25–32 in Ref. 21, and then analyzed in Ref. 22. In Table XI we give the experimental data along with the results of the analysis. The rms radii of the proton distribution (third column) were extracted from data on the isotopic shifts.[91] The analysis in Ref. 22 was performed in the Glauber approximation, using the Fermi representation for the proton and neutron densities and taking into account the data from Ref. 91. Versions (a) and (b) in the table correspond to slightly different choices of the parameters for calculating the densities.

We see that the radii extracted from the experimental data depend weakly on how the densities are parametrized (the maximum difference is about 5% for ^{22}Na). In isotopes with $A=20-22$, $R_{\rm rms}(p)>R_{\rm rms}(n)$, for all the other isotopes $R_{\rm rms}(p)<R_{\rm rms}(n)$, and for ^{31}Na the size of the neutron cloud is 0.305 F in one parametrization and 0.335 F in the other. The size of the neutron cloud therefore turned out to be more sensitive to how the density was parametrized, and it is necessary to include the errors in determining the radii (they are given in parentheses in Table XI). As shown in Ref. 22, the quantity Δr_{np} is correlated with the difference of the proton and neutron separation energies: the larger this difference, the larger the neutron cloud. This correlation was predicted by the relativistic mean-field model.[92] It was first shown in Ref. 22 that the change of $R_{\rm rms}(m)$ for Na isotopes is mainly related to the change of $R_{\rm rms}(n)$.

2.5. Isobars with $A=17$ and $A=20$

Measurements of σ_I for isobars with $A=17$ (^{17}Ne, ^{17}F, ^{17}N, and ^{17}B) at an energy of about 700 MeV/nucleon were made in Refs. 93 and 94, and an anomaly was found for ^{17}Ne and ^{17}B: the cross sections measured for these two nuclei on a carbon target turned out to be considerably larger than for the two other isobars.

The cross sections for isobars with $A=17$ and $A=20$ were analyzed using the Glauber approximation with zero interaction range in Ref. 95. There, with reference to Refs. 96 and 97, it was noted that in the simple Glauber model unitarity and invariance under time reversal are violated. It is stated that these corrections amount to a few percent in the case of the nucleon–nucleus interaction, and may be larger in the nucleus–nucleus case. The results of the analysis[95] are shown in Fig. 12. As indicated in the figure, the densities were calculated by the Hartree–Fock method in the spherical and deformed bases. The calculations for ^{17}Ne (^{17}N) were performed for two variants in the spherical basis, assuming the $1d_{5/2}$ or $2s_{1/2}$ orbitals for the configuration occupied by the last protons (neutrons).

TABLE XI. Interaction cross sections σ_I (mb) and rms radii (F) of the proton, neutron, and matter distributions for Na isotopes.

		Ref. 91	(a)		(b)	
A	σ_I	$\tilde{r}_p$	$\tilde{r}_m$	$\tilde{r}_n$	$\tilde{r}_m$	$\tilde{r}_n$
20	1086(11)	2.806(15)	2.742(28)	2.661(57)	2.729(38)	2.631(80)
21	1100(9)	2.862(12)	2.754(28)	2.630(55)	2.735(38)	2.589(76)
22	1092(16)	2.829(11)	2.730(31)	2.627(59)	2.67(6)	2.51(12)
23	1147(12)	2.829(9)	2.833(23)	2.838(44)	2.819(32)	2.811(60)
25	1185(9)	2.794(10)	2.891(14)	2.965(25)	2.874(18)	2.936(32)
26	1211(16)	2.814(10)	2.934(25)	3.020(45)	2.921(40)	2.998(71)
27	1229(18)	2.836(11)	2.965(32)	3.051(56)	2.946(44)	3.020(77)
28	1265(10)	2.862(12)	3.027(15)	3.129(25)	3.021(12)	3.120(30)
29	1281(22)	2.919(16)	3.053(34)	3.133(57)	3.046(53)	3.121(88)
30	1318(15)	2.942(21)	3.117(24)	3.214(38)	3.119(35)	3.217(57)
31	1358(41)	2.982(14)	3.19(6)	3.29(10)	3.20(8)	3.32(14)
32	1395(61)		3.24(10)	3.36(16)	3.27(15)	3.40(19)

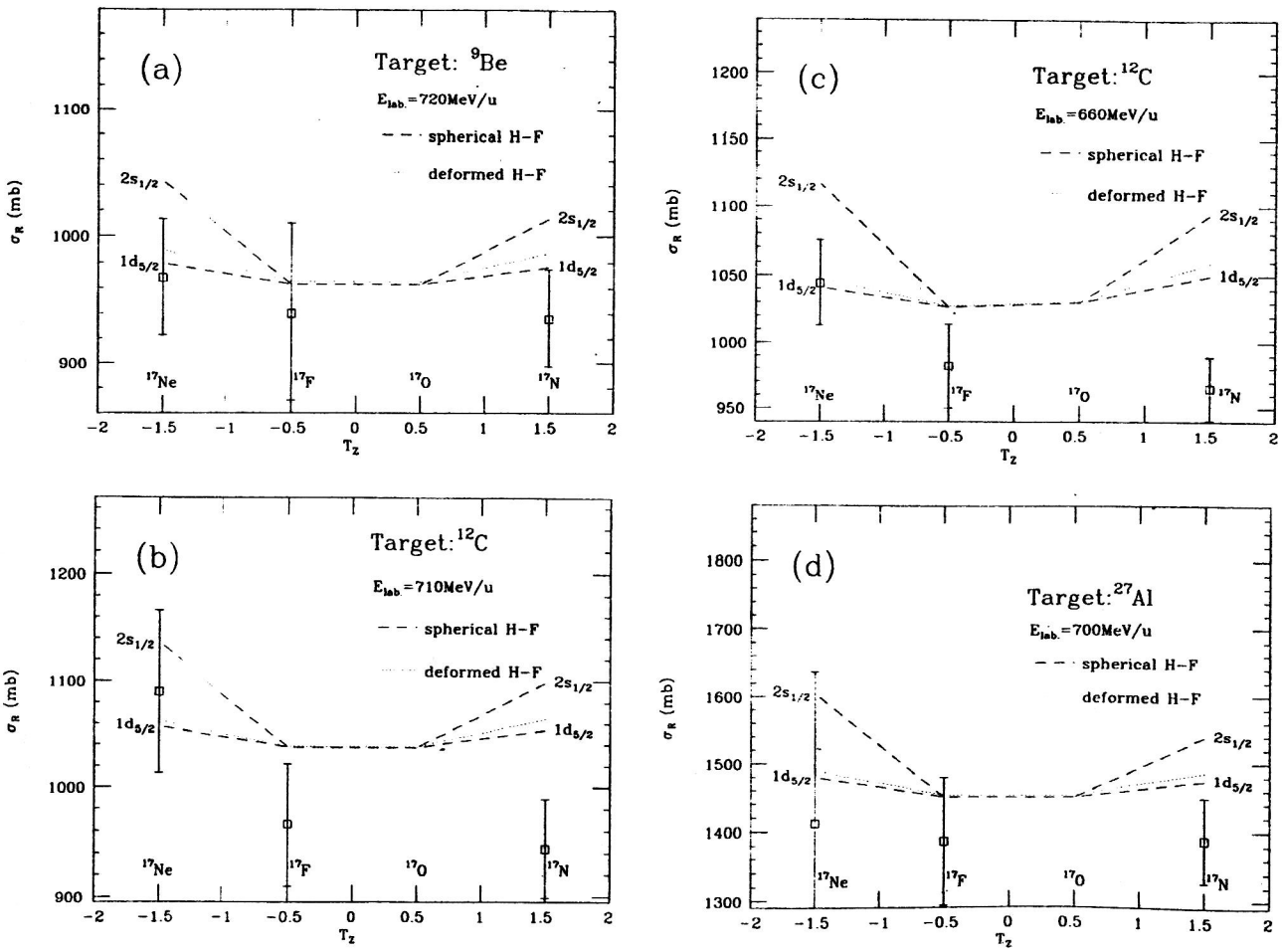

FIG. 12. Total reaction cross sections σ_R, calculated using the densities of the Hartree–Fock method for isobars with $A=17$, and the experimental data.

The results of the calculations[95] in the spherical Hartree–Fock basis with SGII forces are given in Table XII. The energies of the levels of the last occupied orbits for neutrons (λ_n) and for protons (λ_p) are given in the last two columns. The inclusion of deformation effects tends to increase the radii in accordance with the expression

$$\langle r^2\rangle_\beta \simeq \left(1+\frac{5}{4\pi}\beta^2\right)\cdot\langle r^2\rangle_{\beta=0}. \qquad (23)$$

However, it became clear that deformation effects have little influence on the radii, the dominant factor being the neutron excess.

Let us discuss the results of the analysis shown in Fig. 12. It can be seen that for nuclei with isospin $T=\frac{3}{2}$ the use of the $2s_{1/2}$ orbital increases the cross sections by 4–6% compared to the use of the $1d_{5/2}$ orbital, which is due to neutron halo effects. On the whole, the theoretical results describing the behavior of the cross sections as a function of T_z are somewhat higher than the experimental values of σ_I. The authors of Ref. 95 note that the inclusion of breakup effects can lead to a decrease in the calculated values of σ_R and, therefore, to an increase of the radii extracted from experiment.

The cross sections σ_I for isobars with $A=20$ were measured in Ref. 27 at 950 MeV/nucleon on a ^{12}C target. The first analysis of these data using the strong-absorption model with the Kox parametrization and the Glauber approximation was performed in the same study. In the Glauber calculations the densities were parametrized in the harmonic-oscillator representation or as Fermi distributions. The following results were obtained. The largest difference in the radii, equal to 0.2 F, was found for the mirror nuclei ^{20}O and ^{20}Mg. It was suggested that ^{20}Mg has a proton cloud and ^{20}N has a neutron cloud. The largest difference in the radii of the neutron and proton distributions was found for nuclei with large proton excess [^{20}Mg, $\Delta r_{np}=-0.50\pm0.28$ F] and neutron excess [^{20}N, $\Delta r_{np}=0.33\pm0.15$ F]. The choice of density parametrization (the harmonic-oscillator representation or the Fermi distribution) insignificantly (within 1.5–2%) affects the results.

The data from Ref. 27 were also analyzed in Refs. 84 and 95. The results are given in Table XIII together with the experimental data from Ref. 27. In the second and third columns we give the results of the calculations in the spherical and deformed Hartree–Fock bases from Ref. 95, and in the fourth column we give the cross sections σ_R calculated in the semi-microscopic approach with density functional using the Glauber approximation.[84] It can be seen that the use of the deformed basis insignificantly affects σ_R (the maximum change is about 4% for ^{20}Ne), while the agreement with experiment remains unchanged. Both of the theoretical approaches give a fairly good description of the experimental

TABLE XII. Rms radii of the neutron, proton, and matter distributions for isobars with $A=17$ and $A=20$, calculated in the spherical basis of the Hartree–Fock method.

Nucleus	Orbital	r_n (F)	r_p (F)	r_m (F)	λ_n (MeV)	λ_p (MeV)
$^{17}_{5}B_{12}$		2.976	2.452	2.832	−2.85	−20.73
	$(1d_{5/2})^4_\nu(*)$	3.064	2.421	2.890	−0.695	−22.49
	$(2s_{1/2})^2_\nu(*)$	3.623	2.421	3.315	−0.695	−22.49
$^{17}_{6}C_{11}$		2.847	2.488	2.726	−4.12	−23.49
	$(1d_{5/2})^3_\nu(*)$	2.915	2.473	2.764	−0.729	−21.94
	$(2s_{1/2})^1_\nu(*)$	3.221	2.473	2.979	−0.729	−21.94
$^{17}_{7}N_{10}$		2.762	2.563	2.682	−5.67	−15.78
	$(1d_{5/2})^2_\nu(*)$	2.777	2.545	2.684	−4.19	−12.01
	$(2s_{1/2})^2_\nu(*)$	2.902	2.545	2.760	−4.19	−12.01
$^{17}_{8}O_{9}$		2.688	2.631	2.661	−7.23	−13.45
$^{17}_{9}F_{8}$		2.610	2.723	2.670	−16.85	−3.57
$^{17}_{10}Ne_{7}$		2.550	2.819	2.711	−18.72	−1.68
	$(1d_{5/2})^2_\nu(*)$	2.526	2.843	2.717	−15.03	−0.48
	$(2s_{1/2})^2_\nu(*)$	2.526	3.105	2.880	−15.03	−0.48
$^{20}_{6}C_{14}$		2.993	2.526	2.861	−5.15	−28.14
$^{20}_{7}N_{13}$		2.926	2.592	2.813	−6.47	−20.94
$^{20}_{8}O_{12}$		2.869	2.650	2.784	−7.85	−18.64
$^{20}_{9}F_{11}$		2.817	2.726	2.777	−9.10	−8.07
$^{20}_{10}Ne_{10}$		2.764	2.795	2.779	−10.38	−6.36
$^{20}_{11}Na_{9}$		2.705	2.862	2.792	−11.70	−4.71
$^{20}_{12}Mg_{8}$		2.638	2.931	2.818	−21.96	−3.11
$^{20}_{13}Al_{7}$		2.587	3.017	2.874	−23.73	−1.41
^{9}Be		2.343	2.262	2.307	−11.70	−12.62
^{12}C	(**)	2.245	2.400	2.324	−27.26	−14.14
^{27}Al		2.959	2.960	2.960	−14.48	−10.57

data. The values of σ_R obtained using the semi-microscopic approach with density functional are somewhat higher, but the average deviation of the theoretical results from experiment is only 6%. The experimental value of σ_I for ^{20}Na, given in Table XIII, coincides within the error with the corresponding value from Table XI.

CONCLUSION

The cross sections for interactions of light exotic nuclei with stable nuclei have been measured since the very start of the experimental study of the former. The total reaction and interaction cross sections were later obtained for many isotopes of He, Li, Be, B, C, and Na, and also isobars with $A=17$ and $A=20$ at both high (400, 700–950 MeV/nucleon) and intermediate (10–80 MeV/nucleon) energies. Even in the first measurements it was found that the radii of light exotic nuclei have a strong isotopic dependence, and after further studies of fragmentation, dissociation, transfer, etc., reactions it was suggested that these nuclei have a neutron halo (^{11}Li, ^{6}He, ^{11}Be) or, possibly, a proton halo (^{8}B). A significant neutron or proton cloud was found for many nuclei. Interesting regularities in the behavior of the matter distribution radii were revealed in Na isotopes, and also for isobars with $A=17$ and $A=20$.

The experimental data have been analyzed using various approaches, including the strong-absorption model, the standard optical model, the semi-microscopic approach based on the double-folding model, and the Glauber approximation. The strong-absorption model and the standard optical model do not give a completely successful description of the experimental data, and the analyses based on them give only general information about the geometrical properties of nuclei. The use of semi-microscopic approaches like the optical model with microscopic double-folding potentials and the Glauber theory requires the construction of the neutron and proton densities according to specific nuclear-structure models, and therefore allows such models to be tested by analyzing the cross sections.

Various approaches have been used to calculate the nuclear densities: the shell model, the Hartree–Fock method with spherical and deformed bases, the density-functional method, and the cluster approach. It appears most reasonable to use a model in which the neutron and proton densities are calculated within a single scheme for both the target nucleus and the projectile. At present, such a scheme has been realized on the basis of the density-functional method (which is

TABLE XIII. Total reaction cross sections σ_R for isobars with $A=20$, calculated in the Glauber approximation, and experimental interaction cross sections σ_I.

Nucleus	Spherical HF basis	Deformed HF basis	Density-functional method	Exp.
^{20}N	1145	1152	1227	1121(17)
^{20}O	1129	1138	1181	1078(10)
^{20}F	1124	1147	1162	1113(11)
^{20}Ne	1125	1168	1163	1144(10)
^{20}Na	1131	1155	1172	1094(11)
^{20}Mg	1145	1154	1207	1150(12)

actually one version of the self-consistent theory of finite Fermi systems).

The optical limit with zero interaction range of the Glauber theory appears to be a reasonable approximation for analyzing the interaction cross sections at high energies, but at intermediate energies ($E/A \leqslant 100$ MeV/nucleon) it is necessary to include various corrections (the finite interaction range, various nucleon correlations, and noneikonal and Coulomb effects).

At energies of up to 100 MeV/nucleon it is reasonable to use the semi-microscopic optical model, in which the real part of the potential is calculated using some version of the double-folding model, and the imaginary part is parametrized. The calculations of the reaction cross sections in this model can possess predictive power only when the absorption-potential parameters are fixed either by choosing them from known systematics, or by comparing the theoretical angular distributions of elastic scattering with the experimental ones measured at the same energy as the total reaction cross section. The systematics of the absorption-potential parameters for stable nuclei are far from always applicable to exotic nuclei, and so it is extremely desirable to measure simultaneously the angular distributions of elastic scattering and the total reaction cross sections for a single projectile at a given energy. So far such experimental data are rather scarce.

It would be very useful to measure the cross sections σ_R in the energy range 100–200 MeV/nucleon. The Glauber approximation is already valid in this range, and also it is still possible to use the semi-microscopic optical model. Analysis of the experimental data in this range would, on the one hand, allow two semi-microscopic approaches to be compared and, on the other, would supplement the existing analysis of the energy dependence of σ_R.

In conclusion, the authors are grateful to G. D. Alkhazov, A. A. Korsheninnikov, A. A. Ogloblin, Yu. É. Penionzhkevich, and N. K. Skobelev for fruitful discussions about the problems discussed in this review. One of the authors (S. A. F.) thanks D. Zawischa for interesting discussions. This work was carried out with the partial support of the Russian Fund for Fundamental Research (Project No. 98-02-16979) and the German Research Society (DFG).

[1] I. Tanihata, in *Treatise on Heavy-Ion Science*, edited by D. A. Bromley (Plenum, New York, 1989), Vol. 8, p. 443.
[2] C. Detraz and D. J. Vietra, Annu. Rev. Nucl. Part. Sci. **39**, 407 (1989).
[3] E. Roeckl, Rep. Prog. Phys. **55**, 1661 (1992).
[4] C. A. Bertulani, L. F. Canto, and M. S. Hussein, Phys. Rep. **226**, 281 (1993).
[5] K. Riissager, Rev. Mod. Phys. **66**, 1105 (1994).
[6] I. Tanihata, J. Phys. G **22**, 157 (1996).
[7] O. M. Knyaz'kov, I. N. Kukhtina, and S. A. Fayans, Fiz. Élem. Chastits At. Yadra **28**, 1061 (1997) [Phys. Part. Nuclei **28**, 418 (1997)].
[8] I. Tanihata, H. Hamagaki, O. Hashimoto *et al.*, Phys. Lett. B **160**, 380 (1985).
[9] I. Tanihata, H. Hamagaki, O. Hashimoto *et al.*, Phys. Rev. Lett. B **55**, 2676 (1985).
[10] I. Tanihata, T. Kobayashi, O. Yamakawa *et al.*, Phys. Lett. B **206**, 592 (1988).
[11] I. Tanihata, T. Kobayashi, T. Suzuki *et al.*, Phys. Lett. B **287**, 307 (1992).
[12] T. Minamisono, T. Ohtsubo, and I. Minami, Phys. Rev. Lett. **69**, 2058 (1992).
[13] A. C. C. Villari, W. Mittig, E. Plagnol *et al.*, Phys. Lett. B **268**, 345 (1991).
[14] B. Blank, J.-J. Gaimard, H. Geissel *et al.*, Z. Phys. A **340**, 41 (1991).
[15] B. Blank, J.-J. Gaimard, H. Geissel *et al.*, Nucl. Phys. A **555**, 408 (1993).
[16] R. E. Warner, R. A. Patty, P. M. Voyles *et al.*, Phys. Rev. C **54**, 1700 (1996).
[17] R. E. Warner, I. H. Kelley, P. Zecher *et al.*, Phys. Rev. C **52**, R1166 (1995).
[18] F. Negoita, C. Borcea, F. Carstoiu *et al.*, Phys. Rev. C **54**, 1787 (1996).
[19] A. Ozawa, I. Tanihata, T. Kobayashi *et al.*, Nucl. Phys. A **608**, 63 (1996).
[20] M. M. Obuti, T. Kobayashi, D. Hirata *et al.*, Nucl. Phys. A **609**, 74 (1996).
[21] T. Suzuki, H. Geissel, O. Bochkarev *et al.*, Phys. Rev. Lett. **75**, 3241 (1995).
[22] T. Suzuki, H. Geissel O. Bochkarev *et al.*, Nucl. Phys. A **630**, 402c (1998).
[23] N. Alahari, D. Bazin, B. Davids *et al.*, in *Proceedings of the Second International Conference on Exotic Nuclei and Atomic Masses*, June, 1998, Shanty Creek Resort, Bellaire, Michigan, USA, Book of Abstracts, p. B8.
[24] B. A. Brown and P. G. Hansen, Phys. Lett. B **381**, 391 (1996).
[25] I. Licot, N. Added, N. Carlin *et al.*, Phys. Rev. C **56**, 250 (1997).
[26] I. Tanihata, T. Kobayashi, S. Shimoura *et al.*, in *Proceedings of the First International Conference on Radioactive Nuclear Beams*, edited by W. D. Meyers, J. M. Nitschke, and E. B. Norman (World Scientific, Singapore, 1990), p. 429.
[27] L. Chulkov, G. Kraus, O. Bochkarev *et al.*, Nucl. Phys. A **603**, 219 (1996).
[28] R. J. Glauber, in *Lectures in Theoretical Physics*, edited by W. E. Brittin (Interscience, New York, 1959), Vol. 1, p. 315.
[29] S. Kox, A. Gamp, C. Perrin *et al.*, Phys. Rev. C **35**, 1678 (1987).
[30] G. R. Satchler and W. G. Love, Phys. Rep. **55**, 183 (1979).
[31] A. V. Smirnov, S. V. Tolokonnikov, and S. A. Fayans, Yad. Fiz. **48**, 1661 (1988) [Sov. J. Nucl. Phys. **48**, 995 (1988)].
[32] W.-Q. Shen, B. Wang, J. Feng *et al.*, Nucl. Phys. A **491**, 130 (1989).
[33] O. M. Knyaz'kov, Fiz. Élem. Chastits At. Yadra **17**, 318 (1986) [Sov. J. Part. Phys. **17**, 137 (1986)].
[34] Dao Tien Khoa and O. M. Knyaz'kov, Fiz. Élem. Chastits At. Yadra **21**, 1456 (1990) [Sov. J. Part. Phys. **21**, 623 (1990)].
[35] M. Lewitowicz, C. Borcea, F. Carstoiu *et al.*, Nucl. Phys. A **562**, 301 (1993).
[36] M. Zahar, M. Belbot, J. J. Kolata, *et al.*, Phys. Rev. C **49**, 1540 (1994).
[37] M. C. Mermaz, Phys. Rev. C **50**, 2620 (1994).
[38] J. J. Kolata, M. Zahar, R. Smith *et al.*, Phys. Rev. Lett. **69**, 2631 (1992).
[39] S. A. Fayans, O. M. Knyazkov, I. N. Kuchtina *et al.*, Phys. Lett. B **357**, 509 (1995).
[40] Dao Tien Khoa, G. R. Satchler, and W. von Oertzen, Phys. Lett. B **358**, 14 (1995).
[41] F. Carstoiu and M. Lassaut, Nucl. Phys. A **597**, 2213 (1996).
[42] G. R. Satchler, *Direct Nuclear Reactions* (Oxford University Press, New York, 1983).
[43] A. K. Chaudhuri, D. N. Basu, and B. Sinha, Nucl. Phys. A **439**, 415 (1985).
[44] X. Campi and A. Bouyssy, Phys. Lett. B **73**, 263 (1978).
[45] G. F. Bertsch, J. Borysowicz, H. McManus *et al.*, Nucl. Phys. A **284**, 399 (1977).
[46] N. Anantaraman, H. Toki, and G. F. Bertsch, Nucl. Phys. A **398**, 269 (1983).
[47] M. E. Brandan and G. R. Satchler, Phys. Rep. **285**, 143 (1997).
[48] D. V. Bolotov, O. M. Knyaz'kov, I. N. Kukhtina, and S. A. Fayans, Yad. Fiz. (1999) [Phys. At. Nucl.] (in press).
[49] A. M. Kobos, B. A. Brown, P. E. Hodgson *et al.*, Nucl. Phys. A **384**, 65 (1982).
[50] J.-P. Jeukenne, A. Lejeune, and C. Mahaux, Phys. Rev. C **16**, 80 (1977).
[51] S. A. Goncharov, O. M. Knyaz'kov, and A. A. Kolozhvari, Yad. Fiz. **59**, 666 (1996) [Phys. At. Nucl. **59**, 634 (1996)].
[52] S. K. Charagi and S. K. Gupta, Phys. Rev. C **41**, 161 (1990).
[53] G. F. Bertsch, B. A. Brown, and H. Sagawa, Phys. Rev. C **39**, 1154 (1989).
[54] M. A. Franey and W. G. Love, Phys. Rev. C **31**, 488 (1985).
[55] L. Ray, Phys. Rev. C **20**, 1857 (1979).
[56] S. K. Charagi and S. K. Gupta, Phys. Rev. C **56**, 1171 (1997).
[57] J. S. Al-Khalili, J. A. Tostevin, and I. J. Thompson, Phys. Rev. C **54**, 1843 (1996).

[58] R. A. Rego, Nucl. Phys. A **581**, 119 (1995).
[59] F. A. Gareev, S. N. Ershov, G. S. Kazacha *et al.*, Yad. Fiz. **58**, 620 (1995) [Phys. At. Nucl. **58**, 564 (1995)].
[60] S. Yu. Shmakov, V. V. Uzhinskii, and A. M. Zadorozhny, Comput. Phys. Commun. **54**, 125 (1989).
[61] J. S. Al-Khalili and J. A. Tostevin, Phys. Rev. Lett. **76**, 3903 (1996).
[62] G. D. Alkazov, in *Proceedings of the Second International Conference on Exotic Nuclei and Atomic Masses*, June, 1998, Shanty Creek Resort, Bellaire, Michigan, USA, Book of Abstracts, p. B5.
[63] A. G. Sitenko, Ukr. Fiz. Zh. **4**, 152 (1959).
[64] H. Sato and Y. Okuhara, Phys. Rev. C **34**, 2171 (1986).
[65] T. Kobayashi, S. Shimoura, I. Tanihata *et al.*, Phys. Lett. B **232**, 51 (1989).
[66] I. Tanihata, Nucl. Phys. A **488**, 113c (1988).
[67] J. A. Tostevin, R. C. Johnson, and J. S. Al-Khalili, Nucl. Phys. A **630**, 340c (1998).
[68] R. E. Warner, A. M. van den Berg, K. M. Berland *et al.*, Phys. Rev. C **40**, 2473 (1989).
[69] A. Auce, P. F. Carlson, A. J. Cox *et al.*, Phys. Rev. C **50**, 871 (1994).
[70] P. J. Karol, Phys. Rev. C **11**, 1203 (1975).
[71] R. E. Warner and G. N. Felder, Phys. Rev. C **42**, 2252 (1990).
[72] H. Rebel, G. W. Schweimer, J. Specht *et al.*, Nucl. Phys. A **182**, 145 (1972).
[73] B. Tatischeff and I. Brissaud, Nucl. Phys. A **155**, 89 (1970).
[74] G. R. Satchler, Nucl. Phys. A **70**, 177 (1965).
[75] M. G. Saint-Laurent, R. Anne, D. Bazin *et al.*, Z. Phys. A **332**, 457 (1989).
[76] Nguen van Giai and H. Sagawa, Phys. Lett. B **106**, 379 (1981).
[77] N. Takigawa, M. Ueda, M. Kuratani, and H. Sagawa, Phys. Lett. B **288**, 244 (1992).
[78] S. A. Fayans, D. V. Bolotov, O. M. Knyazkov, and I. N. Kuchtina, in *Proceedings of the International School-Seminar on Heavy Ion Physics*, September, 1997, Dubna, Russia, Abstracts, p. 100.
[79] O. M. Knyaz'kov, A. A. Kolozhvari, I. N. Kukhtina, and S. A. Fayans, Yad. Fiz. **59**, 466 (1996) [Phys. At. Nucl. **59**, 439 (1996)].
[80] O. M. Knyaz'kov, I. N. Kukhtina, Yu. É. Penionzhkevich *et al.*, Yad. Fiz. **59**, 1188 (1996) [Phys. At. Nucl. **59**, 1138 (1996)].
[81] O. M. Knyaz'kov, I. N. Kukhtina, and S. A. Fayans, Yad. Fiz. **61**, 603 (1998) [Sov. J. Nucl. Phys. **61**, 533 (1998)].
[82] S. A. Fayans, O. M. Knyazkov, and I. N. Kuchtina, Nucl. Phys. A **626**, 263c (1997).
[83] O. M. Knyaz'kov, I. N. Kukhtina, and S. A. Fayans, Yad. Fiz. **61**, 827 (1998) [Sov. J. Nucl. Phys. **61**, 744 (1998)].
[84] S. A. Fayans, D. V. Bolotov, O. M. Knyazkov, and I. N. Kuchtina, in *Proceedings of the Second International Conference on Exotic Nuclei and Atomic Masses*, June, 1998, Shanty Creek Resort, Bellaire, Michigan, USA, Book of Abstracts, p. PB8.
[85] S. Shimoura, in *Proceedings of the Second International Conference on Radioactive Beams*, edited by Th. Deebar (Adam Hilger, Bristol, 1992), p. 215.
[86] M. Fukuda, T. Ichihara, N. Inabe *et al.*, Phys. Lett. B **268**, 339 (1991).
[87] T. Suzuki, K. Sümmerer, O. Bochkarev *et al.*, in *Proceedings of the Second International Conference on Exotic Nuclei and Atomic Masses*, June, 1998, Shanty Creek Resort, Bellaire, Michigan, USA, Book of Abstracts, p. A12.
[88] I. Pechina, R. Anne, D. Bazin *et al.*, Phys. Rev. C **52**, 191 (1995).
[89] M. Fukuda, M. Mihara, T. Fukao *et al.*, Nucl. Phys. A **630**, (1998).
[90] B. Blank, C. Marchand, M. S. Pravikoff *et al.*, Nucl. Phys. A **624**, 242 (1997).
[91] G. Huber, F. Touchard, S. Büttgenbach *et al.*, Phys. Rev. C **18**, 2342 (1978).
[92] D. Hirata, H. Toki, T. Warabe *et al.*, Phys. Rev. C **44**, 1467 (1991).
[93] I. Tanihata, T. Kobayashi, S. Shimoura *et al.*, in *Proceedings of the First International Conference on Radioactive Nuclear Beams*, edited by W. D. Meyers, J. M. Nitschke, and E. B. Norman (World Scientific, Singapore, 1990), p. 429.
[94] A. Ozawa, T. Kobayashi, H. Sato *et al.*, Phys. Lett. B **334**, 18 (1994).
[95] H. Kitagawa, N. Tajima, and H. Sagawa, Z. Phys. A **358**, 381 (1997).
[96] C. Lazard, R. J. Lombard, and Z. Maric, J. Phys. G **11**, 991 (1985).
[97] C. Lazard, R. J. Lombard, and Z. Maric, J. Phys. G **13**, 321 (1987).

Translated by Patricia A. Millard